RESERVOIR CHARACTERIZATION USING EXPERIMENTAL DESIGN AND RESPONSE SURFACE METHODOLOGY

A Thesis

by

HARSHAL PARIKH

Submitted to the Office of Graduate Studies of
Texas A&M University
in partial fulfillment of the requirements for the degree of

MASTER OF SCIENCE

August 2003

Major Subject: Petroleum Engineering

RESERVOIR CHARACTERIZATION USING EXPERIMENTAL DESIGN AND RESPONSE SURFACE METHODOLOGY

A Thesis

by

HARSHAL PARIKH

Submitted to the Office of Graduate Studies of
Texas A&M University
in partial fulfillment of the requirements for the degree of

MASTER OF SCIENCE

Approved as to style and content by:

Akhil Datta-Gupta (Chair of Committee)	W. John Lee (Member)
Bani K. Mallick (Member)	Hans C. Juvkam-Wold (Head of Department)

August 2003

Major Subject: Petroleum Engineering

ABSTRACT

Reservoir Characterization Using Experimental Design and Response Surface Methodology. (August 2003)

Harshal Parikh, B.S., Mumbai University Institute of Chemical Technology

Chair of Advisory Committee: Dr. Akhil Datta-Gupta

This research combines a statistical tool called experimental design/response surface methodology with reservoir modeling and flow simulation for the purpose of reservoir characterization. Very often, it requires large number of reservoir simulation runs for identifying significant reservoir modeling parameters impacting flow response and for history matching. Experimental design/response surface (ED/RS) is a statistical technique, which allows a systematic approach for minimizing the number of simulation runs to meet the two objectives mentioned above. This methodology may be applied to synthetic and field cases using existing statistical software tools.

The application of ED/RS methodology for the purpose of reservoir characterization has been applied for two different objectives. The first objective is to address the uncertainties in the identification of the location and transmissibility of flow barriers in a field in the Gulf of Mexico. This objective is achieved by setting up a simple full-factorial design. The range of transmissibility of the barriers is selected using a Latin Hypercube Sampling (LHS). An analysis of variance (ANOVA) gives the significance of the location and transmissibility of barriers and comparison with decline-type curve analysis which gives us the most likely scenarios of the location and transmissibility of the flow barriers. The second objective is to identify significant geologic parameters in object-based and pixel-based reservoir models. This study is applied on a synthetic fluvial reservoir, whose characteristic feature is the presence of sinuous sand filled channels within a background of floodplain shale. This particular study reveals the impact of uncertainty in the reservoir modeling parameters on the flow performance.

Box-Behnken design is used in this study to reduce the number of simulation runs along with streamline simulation for flow modeling purposes.

In the first study, we find a good match between field data and that predicted from streamline simulation based on the most likely scenario. This validates the use of ED to get the most likely scenario for the location and transmissibility of flow barriers. It can be concluded from the second study that ED/RS methodology is a powerful tool along with a fast streamline simulator to screen large number of reservoir model realizations for the purpose of studying the effect of uncertainty of geologic modeling parameters on reservoir flow behavior.

DEDICATION

To my beloved parents, my brother, Niraj, and to my lovely fiancé, Sheetal, for their love, care, and inspiration.

ACKNOWLEDGMENTS

I would like to take this opportunity to express my deepest gratitude and appreciation to the people who have given me their assistance throughout my studies and during the preparation of this thesis. I would especially like to thank my advisor and committee chair, Dr. Akhil Datta-Gupta, for his continuous encouragement, financial support, and especially for his academic guidance.

I would like to thank Dr. W. John Lee and Dr. Bani K. Mallick for serving as committee members, and I do very much acknowledge their friendliness, guidance and helpful comments while working towards my graduation.

Finally, I want to thank my friends in the reservoir characterization group, Dr. Arun Khargoria (now with Petrotel), Dr. Zhong He, Dr. Sang Heon Lee (now with ChevronTexaco), Ichiro Osako, Hao Cheng, Ahmed Daoud and Nam Il for making my graduate years very pleasant. The facilities and resources provided by the Harold Vance Department of Petroleum Engineering, Texas A&M University, are gratefully acknowledged. I thank Texas A&M University for educating me in various ways, and for providing me with the very best education there is. I would like to take the opportunity to thank the faculty and staff for helping me prepare for a life after graduation.

I am going to remember these years of hard work with great pleasure. To all of you, I appreciate what you have done to help me in my scholastic and professional growth. I would like to thank you for providing me with a work environment that lends itself to creativity and productivity, without too many financial concerns. Not everyone is so fortunate. I know I still have much to learn, but with continued support and encouragement from people like you I know I can accomplish a great deal.

Thank you very much.

TABLE OF CONTENTS

CHAPTER Page

LIST OF FIGURES

FIGURE Page

LIST OF TABLES

TABLE Page

CHAPTER I

INTRODUCTION - APPLICATION OF EXPERIMENTAL DESIGN/RESPONSE SURFACE METHODOLOGY IN RESERVOIR CHARACTERIZATION

Reservoir characterization is one of the most important phases in reservoir studies. A reservoir model is first developed with static data using a particular type of reservoir modeling technique. Geostatistical simulation is one example for deriving a realistic reservoir description. However, the reservoir modeling parameters are highly uncertain. This leads to an uncertain framework of the reservoir model. Uncertainty in the reservoir model itself introduces an uncertainty in the flow simulation results. As a result it becomes necessary to study the impact of uncertain geologic modeling parameters on the flow performance. However, these kinds of studies typically require a large number of simulation runs. This suggests that it would take too much time to get an accurate description of the reservoir model, rendering the study unfeasible for quick decision making. For that reason, this research proposes to combine flow simulation with a statistical tool called experimental design and response surface methodology (ED/RS). ED/RS reduces the number of simulation runs by intelligently choosing the combinations of reservoir modeling/geologic parameters to change within their uncertainty range.

ED/RS methodology has been previously used in reservoir characterization applications including uncertainty modeling,[1-5] sensitivity studies[1,5] and history matching.[6-9] It has also been widely used in performance predictions within the oil industry.[10-16]

One of the objectives of this thesis was to use experimental design to maximize the information derived from the flow simulation of various geologic models. Previous

---

This thesis follows the style of the *Journal of Petroleum Technology*.

studies have been performed on models generated by pixel-based modeling techniques, which essentially follow variogram-based geostatistical algorithms.[1,3,5] Some studies have also been performed on object-based models.[2,4] This research attempts to assess uncertainty in reservoir modeling parameters for both pixel-based and object-based models under similar geologic settings. This gives an insight into which modeling parameters are significant in both the modeling techniques and gives us a basis to compare the modeling parameters of the two methods. It is shown that the channel permeabilities and the sandstone ratio, which are common modeling parameters in both the cases, have the most significant effect on flow simulation results. Another unique feature of this study is the use of streamline simulation[17] as the flow simulation technique to get the reservoir performance response. This allows fast flow simulation of multiple geologic realizations[18], which is absolutely essential for carrying out such a study requiring large number of simulation runs.

Another important objective was to use ED/RS methodology for history matching purposes.[6-9]. The reservoir is a field case from the Gulf of Mexico. In this study, we utilize ED/RS to identify the most likely location and transmissibility of flow barriers in the reservoir by matching drainage volume from traditional type-curve analysis and from a streamline approach using a diffusive time of flight concept. Then we address the uncertainties in the identification procedure using an experimental design procedure. This gives us the most likely scenario for the location and the transmissibility of the flow barriers. We also compare the bottom hole pressure data with the simulation results. This comparison shows a good match with the field data. This validates the streamline approach used to get drainage volume and the identification of reservoir compartmentalization.

1.1 Experimental Design and Response Surface

Numerical models are widely used in engineering and scientific studies. High performance computers now solve these numerical models. As a result, experimenters have increasingly turned to mathematical models to simulate complex systems. The computer models (or codes) often have high-dimensional inputs, which can be scalars or

functions. The output may also be multivariate. In particular, it is common for the output to be time-dependent function from which a number of summary responses are extracted. Making a number of runs at various input configurations is what we call a computer experiment. The design problem is the choice of inputs for efficient analysis of data. Experimental design is an intelligent way to pick the choice of input combinations for minimizing the number of computer model runs for the purpose of data analysis, inversion problems and input uncertainty assessment. One way to carry the above tasks on experimental design results is to build a response surface. A response surface is an empirical fit of computed responses as a function of input parameters. Another way to do input uncertainty assessment is to perform Analysis of Variance (ANOVA) on the experimental design results.

In experimental design, several parameters are varied simultaneously according to a predefined pattern. The technique gives the possibility of obtaining the same information as the 'one parameter at a time' method with significantly fewer simulation runs, and to obtain some understanding of the possible interactions between the parameters. Experimental Design has been used in diverse areas such as aerospace,[19] civil engineering[20,21] and electronics[22] for analysis and optimization of complex, nonlinear systems described by computer models.[23] As mentioned previously many reservoir engineering studies have used experimental design. For our purpose then, the computer model is essentially a reservoir simulator. The input parameters are classified by our knowledge and our ability to change them. For our cases, we have uncertain geologic or modeling parameters, which can neither be measured accurately nor controlled.

A design is a set of factor-value combinations for which responses are measured.[24,25] For example, in a two-level factorial design, each factor is assigned to its maximum or minimum value (± 1) in all possible combinations with other factors (Fig. 1.1a). For three factors, this requires eight experiments; for k factors, 2^k experiments are needed. Similarly, three-level factorial designs assign each factor its minimum, centerpoint, or maximum value (-1, 0, +1) in all possible combinations with other factors (Fig. 1.1b); this design requires 27 experiments for three factors, or 3^k experiments for k factors.

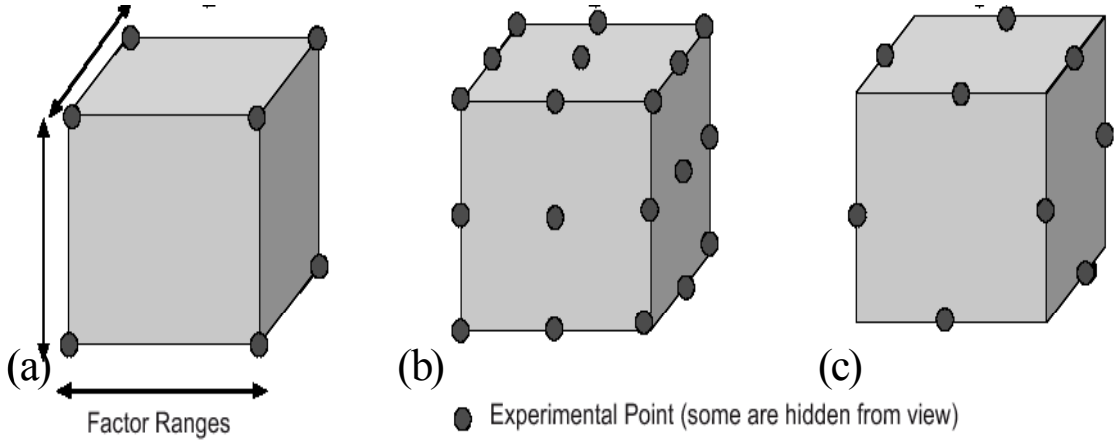

Figure 1.1 – Examples of designs for three factors. (a) A two-level factorial requires eight experiments, (b) a three-level factorial design requires 27 experiments, and (c) a Box-Behnken design requires 15 experiments (including three replicates at the centerpoint).

From the above discussion it is clear that it would take a prohibitively large number of experiments with an increase in the number of factors. Hence we use modified three-level factorial designs, which reduce the number of experiments by confounding higher order interactions. The reduction becomes more significant as the number of factor increases. For the purpose of the first study, which is to identify the most likely scenario for the location and transmissibility of flow barriers, we use a full factorial experimental design since we have just two factors. Then we perform ANOVA on the flow simulation results to analyze the experimental design. For the second study, which is to identify significant geologic modeling parameters and to study their uncertainty impact on flow behavior, we use a Box-Behnken[26] design since we have four factors or geologic modeling parameters. A Box-Behnken design requires less number of experiments as compared to a full-factorial design. For example this design requires 15 experiments for three factors, including three at the factor centerpoint (all factors assigned to their centerpoint values) (Fig.1.1c). Centerpoint replicates make the design more nearly orthogonal, which improves the precision of estimates of response surface coefficients. Also, there is no simple formula relating the number of required experiments to the

number of factors for Box-Behnken designs. Using fast streamline simulation technology on realizations within each scenario of the experimental design, we can get the flow responses. These results allow us to build a response surface model which is an empirical fit of the flow response as a function of the modeling parameters. A Box-Behnken design would give us a second-degree polynomial response surface model. Box-Behnken designs neither require nor depend on the prior specification of the model. Also by including the centerpoint, Box-Behnken designs reduce estimation error for the most likely responses. Analysis of the response surface model would then help to meet our objectives.

1.2 Identification of Most Likely Reservoir Scenario

Reservoir compartmentalization can have a significant impact on the field development. Pressure discontinuities and well production histories can provide important evidence of reservoir compartmentalization in oil and gas reservoirs. The presence of faults or low-permeability barriers produces poor fluid communication between the compartments. This has a significant influence on the depletion performance of the wells. Previous efforts on the study of compartmentalized reservoirs focussed primarily on the modeling of production performance from compartmentalized systems. Such reservoirs have been commonly modeled using material balance techniques, [27-30] although some models have also taken into account transient flow within compartments.[31, 32] All these models require prior knowledge of reservoir compartmentalization and flow barriers. However, such information may not be available, particularly in the early stages of field development with limited geologic and well information. Therefore it is necessary to find a technique to identify reservoir compartmentalization and flow barriers from well production, particularly from primary production.

The approach to identify reservoir compartmentalization and flow barriers utilizes streamline-based drainage volume computations during primary production. Firstly, a decline type curve analysis of the primary production data is used to identify well communications and estimate the drainage volume of individual wells. Second, starting with a geological model the drainage volumes of each well are recomputed using a

streamline-based flow simulation. Reservoir compartmentalization and flow barriers are then inferred through a matching of the streamline-based drainage volume with those from the decline-curve analysis. The role of experimental design is useful in this matching process.

Thus the basic principle involves reconciling reservoir drainage volumes derived from decline curve analysis of primary production response with the drainage volumes computed using a streamline model. The major steps are outlined below.

- Well drainage volume from decline-type curve analysis:

This step involves a conventional decline type-curve analysis whereby the field data is plotted on a log-log plot of normalized production rate, $q/\Delta P$, versus a material balance time, Np/q and then matched with the decline type curves.[33-34] This matching yields the drainage volume associated with the producing well. A deviation of the data from the type curve can be indicative of a drainage volume change resulting from, for example, a new well sharing the drainage volume of the existing well and also indicates pressure communication between the two wells. The deviated data can be rescaled to estimate the new drainage volume associated with each well.

- Well drainage volume from streamline simulation:

Streamline models can be utilized to compute drainage volumes during primary depletion or compressible flow by utilizing the concept of a 'diffusive' time of flight.[35] The 'diffusive' time of flight is associated with the propagation of a front of maximum pressure drawdown or buildup associated with an impulse source/sink and can be used to determine the drainage volumes in 3D heterogeneous media with multiple wells under very general conditions.

- Drainage volume matching to infer the location of flow barriers:

This step reconciles the two drainage volumes for each well: one from decline type curve analysis and other from streamline simulation using the geologic model. Discrepancy between them can suggest the presence of flow barriers that are not included in the geologic model. Different locations and transmissibilities of the flow barriers will give different drainage volumes for the wells. The plausible choice of

locations and the transmissibilities are determined by matching the drainage volumes from streamline simulation with those derived using decline type-curve analysis.

- Quantifying uncertainties via experimental design:

The locations and transmissibilities of flow barriers cannot be uniquely determined without additional information. Thus, we carry out a statistical experimental design to account for their variability and compute the corresponding changes in the drainage volume from streamline simulation. The experimental design allows changing the barrier locations and transmissibilities in a systematic way for matching the drainage volume. Based on the drainage volume matching it is possible to get the most likely scenario for the location and transmissibilities of flow barriers. The final step is to then compare the plot of the observed with the calculated well bottomhole pressure (obtained by performing streamline simulation on the most likely scenario). Also, to determine the relative impact of the locations and transmissibilities of the flow barriers, an analysis of variance (ANOVA) is performed on the experimental design results.

1.3 Uncertainty Analysis of Reservoir Modeling Parameters

Stochastic simulation techniques can be grouped into two main classes of object-based and pixel-based techniques. Geological uncertainties are associated with each technique. These uncertainties in the geological data for each technique are used to constrain the reservoir models. To quantify the significance of a particular geologic factor in each modeling method, an experimental design set-up is used. In this case, a Box-Behnken design is used to get the factor combinations for each experiment.

Reservoir sweep efficiency is used as the response variable. The sweep volume efficiency is obtained using streamline flow simulation. Streamline simulation is used since it is faster than conventional finite-difference simulation and one can easily obtain the swept volume for waterflood cases from streamline simulation computations. The flow simulation result for each experiment helps to build a response surface. The response surface quantifies the importance of a particular geologic factor on the response variable and allows studying the impact of uncertainty in the geologic parameters on the flow behavior of the reservoir. Note that the above procedure is performed on both

modeling methods. The response surfaces for the models from both the methods are then used as a tool to compare the geologic factors from both the methods.

This study is applied on a synthetic fluvial reservoir, whose characteristic feature is the presence of sinuous sand filled channels within a background of floodplain shale. The reservoir models and the modeling parameters to be analyzed for each method are described below:

- Object-based models

A hierarchical object-based modeling of complex fluvial facies is used to model this synthetic reservoir.[36] The task is carried out by FLUVSIM: a program for object-based stochastic modeling of fluvial depositional systems.[37]

Within a layer, the distribution of channel complexes is modeled to honor well data. Facies for each layer is specified for each well as the well data. In the model, three facies are present. The first facies type is background floodplain shale, which is viewed as the matrix within which the sand objects are embedded. The second facies type is channel sand that fills sinuous abandoned channels. This facies is viewed as the best reservoir quality due to the relatively high energy of deposition and consequent coarser grain. The third facies type is levee sand formed along the channel margins. These sands are considered to be poorer quality than the channel fill. For the object-based models the effect of uncertainty of the following geologic modeling parameters is investigated:

1. Channel Dimensions
   - Thickness
   - Width/Thickness Ratio
2. Sandstone ratio
3. Channel Permeability
   - Channel sand permeability
   - Levee sand permeability
4. Channel Sinuosity

The ED/RS methodology would give which parameters from the above are significant and how these parameters affect the volumetric sweep efficiency, which represents the flow performance of the reservoir.

- Pixel-based models

Sequential Indicator Simulation (SIS) is used for the stochastic modeling of fluvial depositional systems. The task is carried out by SISIM provided in GSLIB package. SIS is one of the most popular pixel-based simulation methods and has been proven effective in many case studies

The well data in this case are permeability values for each layer indicating the type of facies for that layer. The type of facies considered here for each layer are similar to those taken for object-based modeling. In this study the effect of uncertainty of the following geologic modeling parameters is investigated:

1. Variogram range
   - Major axis
   - Minor axis
2. Sandstone Ratio/Sandstone pdf cut-off
3. Channel Permeability
   - Channel sand permeability
   - Levee sand permeability
4. Variogram parameters
   - Nugget
   - Sill

Again, the ED/RS methodology would give which parameters from the above are significant and how these parameters affect the volumetric sweep efficiency, which represents the flow performance of the reservoir.

After the above analysis, it is also interesting to compare the modeling parameters for both the methods from the response surface results.

CHAPTER II

EVALUATING UNCERTAINTIES IN IDENTIFICATION OF LOCATION AND TRANSMISSIBILITY OF FLOW BARRIERS

In this chapter, we discuss the application of experimental design in evaluating uncertainties in identification of location and transmissibility of flow barriers. The analysis is performed on a field example in Gulf of Mexico. It has a single well producing under primary depletion. The production rate and flowing bottomhole pressure are monthly averaged. In this chapter, the first part discusses the underlying mathematical formulation behind the drainage volume calculations using the decline type-curve analysis and the concept of streamline 'diffusive' time-of-flight and its relationship with reservoir drainage volumes. The second part would discuss the use of experimental design and analysis of variance to address the uncertainties in the identification procedure.

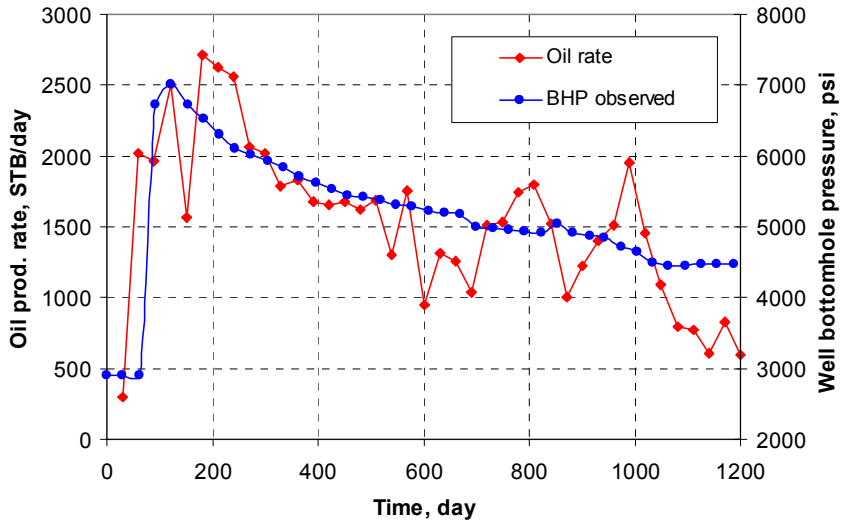

Figure 2.1 – Well production rate and flow bottomhole pressure of the production well for the field case.

2.1 Well Drainage Volume

The analysis is performed on a field example in Gulf of Mexico. It has a single well producing under primary depletion. The production rate and flowing bottomhole pressure (Fig. 2.1) are monthly averaged.

2.1.1 Drainage Volume From Decline Type-Curve

Consider an unfractured well producing a slightly compressible liquid in a closed system under pseudo-steady state flow conditions (boundary dominated flow). The following relationship can be obtained between a normalized flow rate vs. a 'material balance time': [33,34]

$$\frac{q}{p_i - p_{wf}} b_{pss} = \frac{1}{1 + \frac{\overline{B}_o}{NB_{oi}c_e b_{pss}} \bar{t}} \tag{1}$$

where,

$$b_{pss} = \frac{141.2\overline{B}_o\mu_o}{k_o h}\left[\frac{1}{2}\ln\left(\frac{4}{e^{\gamma}}\frac{A}{C_A r'^2_w}\right)\right] \tag{2}$$

$$\bar{t} = \frac{N_p}{q} \tag{3}$$

In dimensionless form Eq. (1) can be expressed as,

$$q_{Dd} = \frac{1}{1 + t_{Dd}} \tag{4}$$

where,

$$q_{Dd} = \frac{141.2\overline{B}_o\mu_o}{k_o h}\left[\frac{1}{2}\ln\left(\frac{4}{e^{\gamma}}\frac{A}{C_A r'^2_w}\right)\right]\frac{q}{p_i - p_{wf}} \tag{5}$$

During decline type curve analysis, a log-log plot of q/ΔP versus $\bar{t}$ on type curves of q_{Dd} versus $\bar{t}_{Dd}$ are overlaid. For our case, type curves have also been generated using flow rate integral and flow rate integral derivative. A simultaneous match to all the three type curves can reduce the subjectivity and personal bias during the matching process.[33, 34] Once the match is obtained the drainage volume can be calculated as follows:

$$N = \frac{B_o}{B_{oi}}\frac{(\bar{t})_{M.P.}}{(t_{Dd})_{M.P.}}\frac{(q_o/\Delta p)_{M.P.}}{(q_{Dd})_{M.P.}} \tag{6}$$

where M.P. refers to match point value.

If there is aquifer support, the expansion of the aquifer can be incorporated into the drainage volume calculations as follows,

$$N_{psd} = N + N_w\frac{B_w}{B_o}\frac{c_a}{c_e} \tag{7}$$

where,

$$\begin{aligned} c_a &= c_f + c_w \\ c_e &= (c_f + c_o s_o + c_w s_w)/s_o \end{aligned} \tag{8}$$

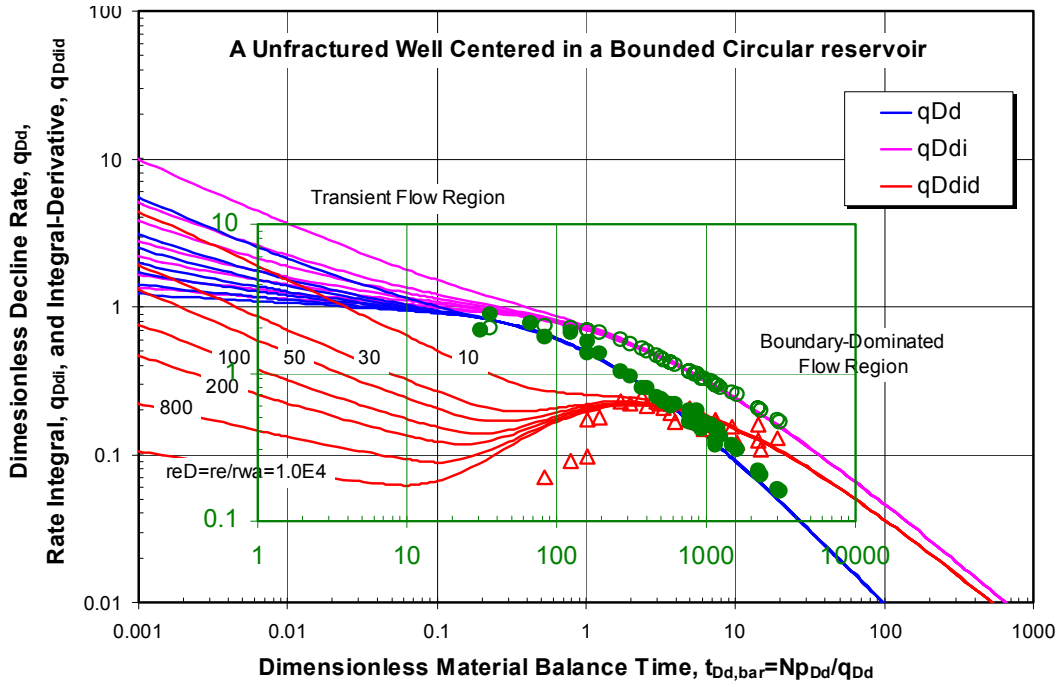

Figure 2.2 – Decline type-curve matching of production well.

A deviation from the type-curve may occur if a new producing well shares the original drainage volume of an existing well. Also, other factors such as multiphase flow can result in a deviation from the type curve because water breakthrough and/or gas production may significantly alter the mobility term and/or total compressibility.

Our aim is to identify reservoir compartmentalization and flow barriers using three years of primary production response. Fig. 2.2 shows the decline type-curve matching. The data follows the type curves pretty well. However the late-time data appears to systematically fall above the type-curves and runs parallel to the type-curve. This indicates a new pseudo-steady state. Such a trend may indicate an extension of the drainage volume. In other words, it may suggest the presence of partially sealing flow barriers that provide production and pressure support at later times via access to additional reservoir volume (compartments). From the decline-curve matching, the estimate of an initial drainage volume is 10.77 MMSTB, and an extended total drainage

volume of 12.43 MMSTB based on the type-curve matching of late-time data points (Fig. 2.3).

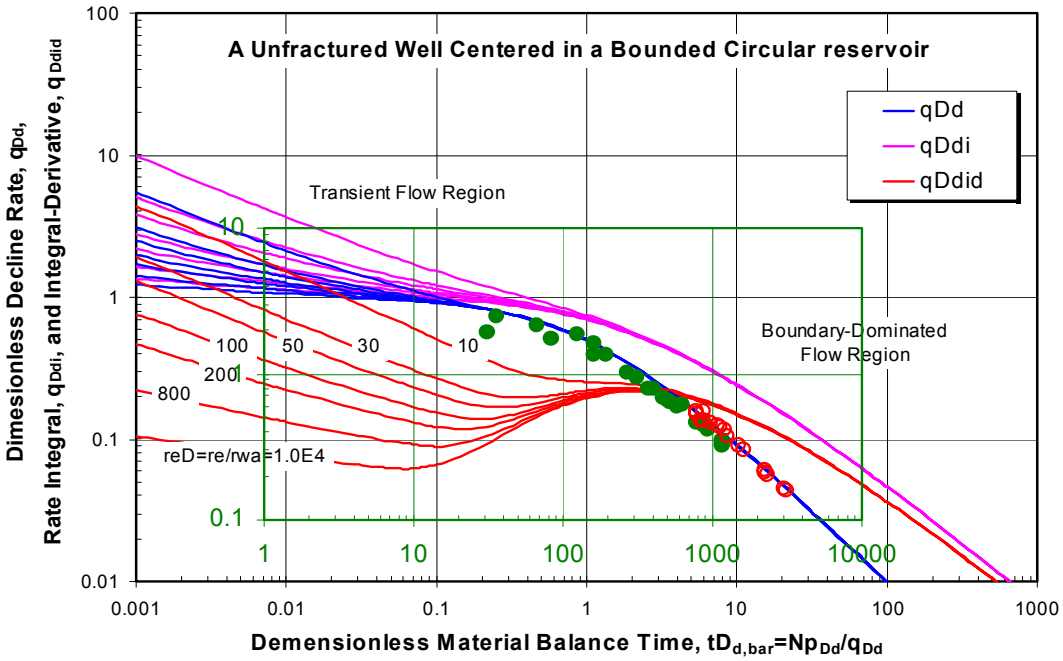

Figure 2.3 – Decline type-curve matching of late-time data points.

2.1.2 Drainage Volume From Streamline 'Diffusive' Time of Flight

The streamline 'diffusive' time of flight concept is based on a high frequency asymptotic solution to the diffusive pressure equation and leads to an equation for a propagating pressure front that is analogous to the 'Eikonal' equation in wave propagation and seismic tomography, as given below

$$\sqrt{\alpha(x)}\left\|\nabla \tau'(x)\right\| = 1 \tag{9}$$

where α is the diffusivity,

$$\alpha(x) = \frac{K(x)}{\phi(x)\mu c_t} \tag{10}$$

From Eq. 9, the pressure front propagates at a velocity given by the square root of diffusivity. The Eikonal equation, being a hyperbolic equation, allows us to invoke characteristic directions and streamlines for propagating fronts. In particular, we can now define a 'diffusive' time of flight for compressible flow as follows,

$$\tau'(x) = \int_{\psi} \frac{ds}{\sqrt{\alpha(x)}} \tag{11}$$

where ψ refers to as streamline and s is the distance along the streamline. Note that the 'diffusive' time of flight has units of square root of time, which is consistent with the scaling behavior of diffusive flow.

It is important to point out that for compressible flow, pathlines can be generated in the same manner as in conventional streamline simulation using the Pollock algorithm.[38] Fluid compressibility acts as a diffusive source (as opposed to a point source) and the semi-analytic pathline construction applies under such conditions.

An important feature of the 'diffusive' time of flight is that it is related to the propagation of a 'pressure front' of maximum drawdown or build up corresponding to an impulse source or sink. This becomes apparent when we examine the time domain solution to the 0^{th} order asymptotic expansion for an impulse source in a three-dimensional medium,[39]

$$P(t) = A_0(x)\frac{\tau'(x)}{2\sqrt{\pi t^3}}\exp\left(-\frac{\tau'^2(x)}{4t}\right) \tag{12}$$

At a fixed position, x, the pressure response, P(t), will be maximized when its derivative is set equal to zero, which in turn results in the following relationship between the observed time and the 'diffusive' time of flight

$$t_{\max} = \frac{\tau'^2(x)}{6} \tag{13}$$

Therefore, the 'diffusive' time of flight is associated with the propagation of a front of maximum drawdown or build up. The time at which the pressure response reaches a maximum at a location for an impulse input can be defined as the transient pressure front arrival time. In fact, this front location is closely related to the concept of drainage volume and drainage radius during conventional well test and decline type curve analysis. For the field case, the reservoir model has 77x55x20 grid cells and was constructed using well log and seismic data. Figs. 2.4-2.5 show the permeability and porosity distribution in the reservoir. The OOIP was calculated to be 16.24 MMSTB resulting in large discrepancy between the volumes from the decline-type curve analysis and that from the reservoir model.

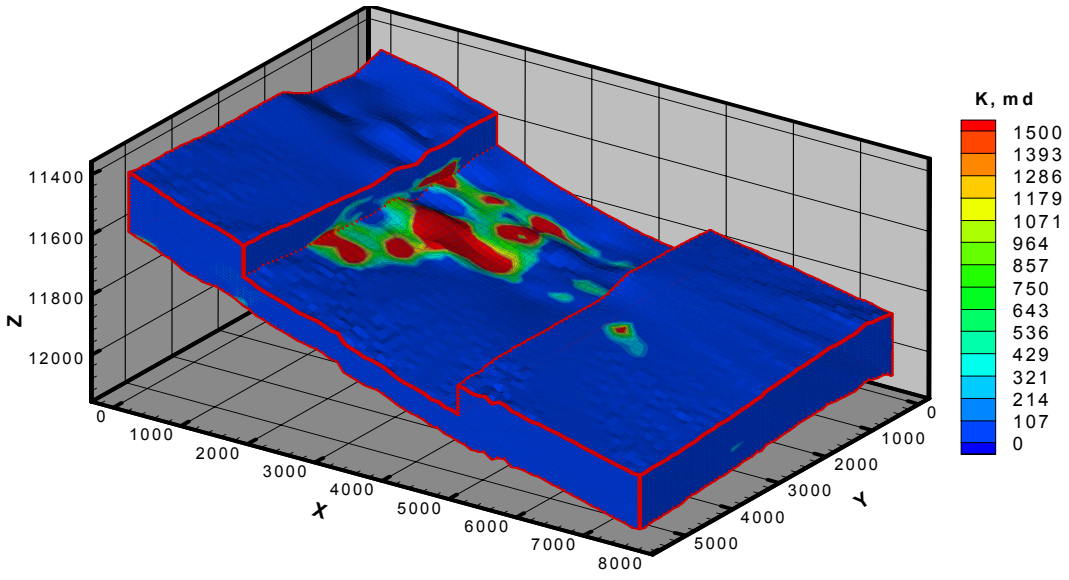

Figure 2.4 – Permeability model of the field.

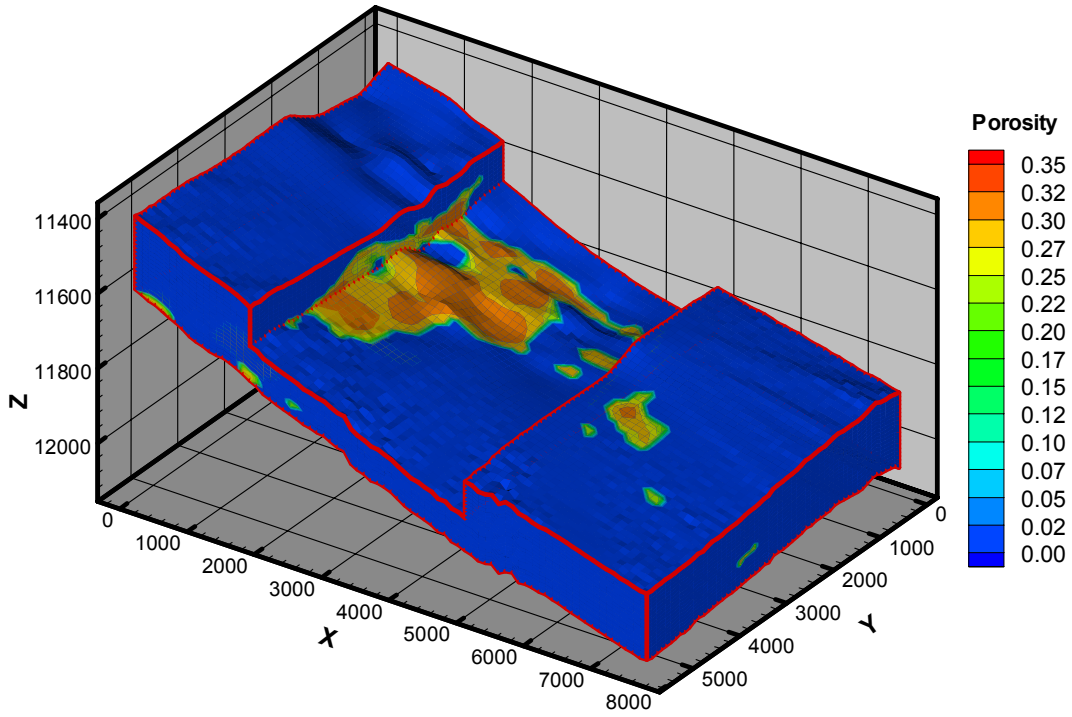

Figure 2.5 – Porosity model of the field.

2.1.3 Drainage Volume Matching

The large discrepancy between the drainage volume from the decline type-curve analysis and that from the reservoir model indicates that a sealing flow barrier prevents the well from draining the whole reservoir. Furthermore, based on the decline type-curve analysis, there may also be a partially sealing flow barrier isolating a portion of the reservoir from the main reservoir. To locate the potential flow barriers, we examine the distributions of permeability, porosity and oil-footage ($\phi * h * S_o$) in the reservoir model for potential trends. Based on low permeability and oil-footage combined with geological input, we place two flow barriers into the reservoir model (Figs. 2.6-2.7) – a northwest barrier and a south barrier. We then proceed to investigate the impact of these flow barriers on the drainage volume calculations using streamline simulation.

Several scenarios are investigated with respect to the location and transmissibilities of flow barriers. To start with, we varied the location of the south barrier while assuming

both the barriers to be almost sealing. The results are shown in Table 1 and Fig. 2.8. We then studied the sensitivity of the NW barrier transmissibility on the drainage volume. The results are shown in Table 2.

Recognizing the non-uniqueness and uncertainty associated with our analysis, we further investigate the barrier location and transmissibility via a statistical experimental design.

Table 1 – Comparison of drainage volume for different locations of the south barrier

	Location	Trans Multiplier	Streamline simulation	Decline type-curve
			Pseudo Drainage Oil Volume, Npsd, Million STB	Pseudo Drainage Oil Volume, Npsd, Million STB
Case 1	No flow barrier	/	18.2	10.77 ~ 12.43
Case 2	South, J=30	0.0001	10.3 ~ 14.6	
	NW	0.0001		
Case 3	South, J=28	0.0001	10.4 ~ 12.8	
	NW	0.0001		
Case 4	South, J=26	0.0001	10.2 ~ 12.4	
	NW	0.0001		

Table 2 – Comparison of drainage volume for different transmissibility multipliers for the NW barrier

	Location	Trans Multiplier	Streamline simulation	Decline type-curve
			Pseudo Drainage Oil Volume, Npsd, Million STB	Pseudo Drainage Oil Volume, Npsd, Million STB
Case 4	South, J=26	0.0001	10.2 ~ 12.4	10.77 ~ 12.43
	NW	0.0001		
Case 5	South, J=26	0.0001	10.0~12.7	
	NW	0.001		
Case 6	South, J=26	0.0001	10.0~13.7	
	NW	0.01		
Case 6	South, J=26	0.0001	10.0~13.7	
	NW	0.1		

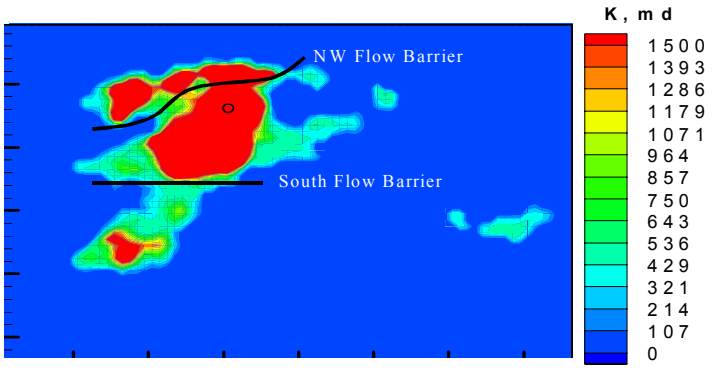

Figure 2.6 – Permeability of layer 10 and potential flow barriers.

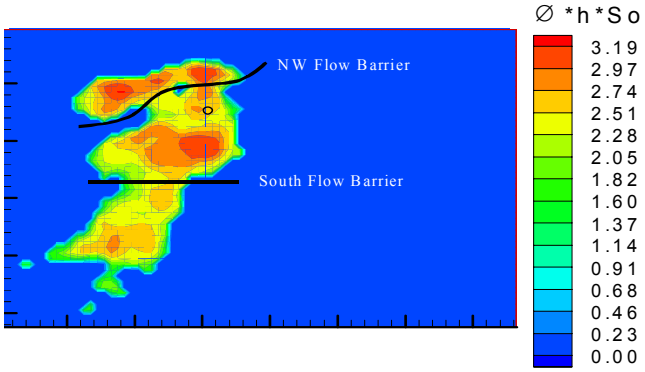

Figure 2.7 – $\phi * h * S_o$ of layer 10 and potential flow barriers.

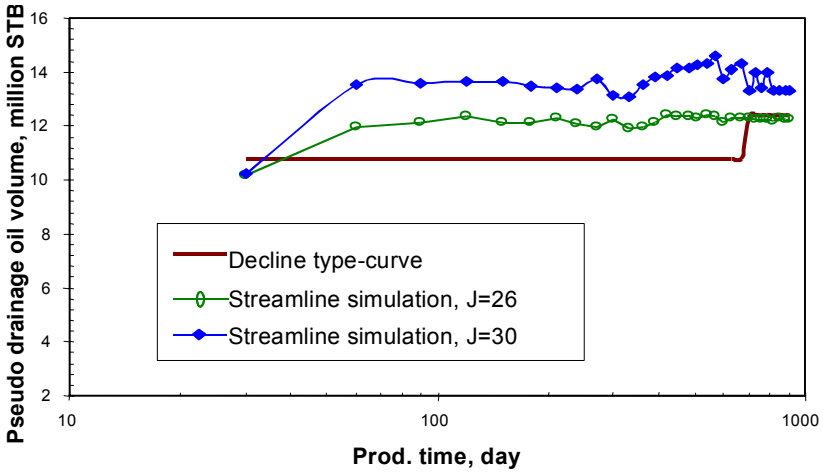

Figure 2.8 –Drainage volume matching for different south barrier locations.

2.2 Quantifying Uncertainties via ED

Experimental Design study would be useful to further validate the approach of the 'diffusive' time of flight concept to compute drainage volume. The study helps us to understand how the uncertainty in the location and transmissibility of flow barriers affects our simulated drainage volume results. It also gives the most probable location and transmissibilities of flow barriers.

In this case, we have two uncertain input parameters; namely, the location of the south barrier and the transmissibilities of the North-west and South flow barriers. The transmissibilities of both the barriers are clubbed as a single parameter. Also, the location of the North-west barrier is considered to be fixed in the simulator. This is because the location of the North-west barrier is known in the geologic model. The different scenarios for the location of the south barrier range from J=22 to J=28. The transmissibilities of the two barriers are combined to give ten levels of the transmissibility parameter. The transmissibility values for each barrier are chosen from a given range using Latin Hypercube sampling (LHS).[40] A full-factorial design is used and an Analysis of Variance (ANOVA) is performed on the experimental design results to fulfill the above mentioned objectives.

2.2.1 Full Factorial Design and LHS

A full-factorial design of experiment measures the response of every possible combination of factor levels. These responses are analyzed, to provide information about main effects, using ANOVA.

Table 3 shows the two factor ranges. The range of the location of south barrier varies from J=22 gridblock in the Y-direction to J=28 gridblock in the Y-direction. The second factor X is a combination of transmissibilities of the two barriers. This factor has ten levels. The individual value of transmissibilities are sampled using LHS from 10 stratified ranges, for each barrier. Then, transmissibilities, randomly picked for the barriers, are paired randomly with each other to give ten levels of the factor X. The assumption inherent in taking 10 levels for transmissibility calculations is that, the ten pairs would represent all the transmissibility combination scenarios possible.

For our case, we assume the range of transmissibility to be uniform. Hence the LHS reduces to stratified random sampling from 10 small ranges obtained by dividing each transmissibility range into 10 equally probable ranges. Table 4 shows the 10 equiprobable ranges for the south (NV1) and north-west transmissibilities (NV2) and the randomly sampled transmissibility values from each range. Table 5 then shows the various combinations of transmissibilities (X1 through X10) of the two barriers obtained by pairing the random samples for each transmissibilities randomly. Once the values of transmissibilities for the 10 levels are fixed, we are ready to perform the experimental design. Table 6 shows the full factorial design along with the streamline simulation results of drainage volume for each factor combination. The simulation is production rate constrained and the production data itself is used as a constrain to simulate the bottomhole pressure data for each scenario.

Table 3 – Factor ranges

Index	Factor Name	Factor Range
1	Location, J	22 - 28
2	Transmissibility	
	South Flow Barrier, NV1	0.00001-1
	Northwest flow barrier,NV2	0.00001-1

Table 4 – Equiprobable ranges for the south and northwest transmissibilities

Range (NV1)	NV1	NV2	Range (NV2)
0.00001-0.00005	0.00001	0.00002	0.00001-0.00005
0.00005-0.0001	0.00006	0.00006	0.00005-0.0001
0.0001-0.0005	0.000313	0.000198	0.0001-0.0005
0.0005-0.001	0.000605	0.000561	0.0005-0.001
0.001-0.005	0.001192	0.001488	0.001-0.005
0.005-0.01	0.006155	0.008966	0.005-0.01
0.01-0.05	0.019242	0.02569	0.01-0.05
0.05-0.1	0.070928	0.061225	0.05-0.1
0.1-0.5	0.489322	0.13699	0.1-0.5
0.5-1	0.502976	0.589651	0.5-1

Table 5 – Transmissibility multipliers of the south and NW barriers obtained using Latin Hypercube Sampling

NV1	NV2	
0.00001	0.58965	X1
0.00031	0.02569	X2
0.07093	0.13699	X3
0.00616	0.00002	X4
0.01924	0.00056	X5
0.00119	0.00006	X6
0.48932	0.0002	X7
0.0006	0.06122	X8
0.00006	0.00897	X9
0.50298	0.00149	X10

Note: NV1 for NW barrier; NV2 for south barrier

Table 6 – Experimental design set-up for drainage volume from streamline simulation for different scenarios

South Barrier Location	X1	X2	X3	X4	X5	X6	X7	X8	X9	X10
	Drainage Volume (Million STB)									
J=22	16.92	16.89	18.19	11.24	12.45	10.57	10.81	17.02	16.51	15.72
J=23	17.05	16.89	18.18	11.18	14.17	11.03	12.07	17.04	16.68	15.74
J = 24	16.94	16.89	18.19	12.89	13.89	11.03	13.03	17.02	16.71	16.84
J = 25	17.10	16.94	18.18	13.31	13.89	12.35	13.37	17.03	16.84	15.33
J = 26	16.93	16.92	18.17	13.54	13.94	12.99	13.54	17.03	16.47	15.18
J = 27	16.98	16.91	18.19	13.71	14.18	13.29	13.88	17.03	16.43	14.74
J = 28	17.05	16.92	18.17	13.93	14.47	13.41	13.98	17.04	16.47	14.99

2.2.2 Analysis of Variance

Based on the experimental design results, we performed an analysis of variance (ANOVA) to examine the significance of the location of the south barrier and the transmissibility of both the barriers on the computed drainage volume. The ANOVA also included the SNK test and Tukey test.[41]. The following equations give the sum of squares computed in the ANOVA

$$SSY = \sum_i \sum_j (y_{ij} - \bar{y})^2 \tag{14}$$

$$SSTrans = \sum_j (\bar{y}_{.j} - \bar{y}_{..})^2 \qquad j = 1,2,....10 \tag{15}$$

$$SSLoc = \sum_i (\bar{y}_{i.} - \bar{y}_{..})^2 \tag{16}$$

$$SSError = SSY - SSTrans - SSLoc \tag{17}$$

$$MSTrans = \frac{SSTrans}{DF}, MSLoc = \frac{SSLoc}{DF}, MSError = \frac{SSError}{DF} \tag{18}$$

where, i= number of the location factor and j= number of transmissibility factor and y_{ij}= drainage volume at i location and j transmissibility, $\bar{y}$ =overall drainage volume, $\bar{y}_{..}$ = sum of drainage volume means

The test of equal transmissibility means, which indicates no transmissibility effects on drainage volume, is a test of,

$$\bar{y}_{.1} = \bar{y}_{.2} = ... = \bar{y}_{.10} \tag{19}$$

The test of equal location means, which indicates no location effects on drainage volume, is a test of,

$$\bar{y}_{.1} = \bar{y}_{.2} = ... = \bar{y}_{.7} \tag{20}$$

The test statistic for testing the above two null hypotheses is,

$$F = \frac{MSTrans}{MSError}, F = \frac{MSLoc}{MSError} \tag{21}$$

which has F distribution with nine (10-1=9) degrees of freedom for MSTrans, six (7-1=6) degrees of freedom for MSLoc and fifty-four (9x6=54) degrees of freedom for the denominator MSError. The analysis of variance (ANOVA) is actually a hypothesis test with the null hypothesis (Ho) that the factor (in our case, transmissibility or location) has no effect on the simulator output (drainage volume in our case). The test statistic (F) in an ANOVA is a Fisher distributed random variable with a certain number of degrees of freedom. A large value on the observed test statistic (Fobs) indicate that the factor has no effect. The Pr-significance value is defined as the probability of having a test statistic that is at least large as the observed test statistic:

$$P = P(F \geq F_{obs} \mid null \cdot hypothesis \cdot is \cdot true) \tag{22}$$

A small Pr-value means that the probability of getting the observed test statistic, given that the null hypothesis is true, is very unlikely. The null hypothesis is then rejected, and we assume that the factor has an effect. That means that the lower the P-significance value, the more significant is the difference amongst different factor level mean responses, indicating that the effect for that particular factor is significant. Table 7 shows the ANOVA table for the experimental design. The table shows the P-significance value for the null hypothesis test. From Table 7 it can be seen that transmissibility of flow barriers have a significant effect on the drainage volume as compared to the location of south barrier.

Table 7 – Analysis of Variance (ANOVA)

Source	DF	Type III SS (SS)	Mean Square (MS)	F Value	Pr
TRANS	9	296.9466	32.9941	79.32	<.0001
LOCATION	6	7.5565	1.2594	3.03	0.0126
Error	54	22.4607	0.4159		

When an ANOVA F test reveals significant differences among the each factor level means (as it did in our case), it does not in any way indicate which means differ or the magnitude of the difference. Thus, the detection of magnitude of difference between factor or level means will require some kind of post-ANOVA analysis. SNK/Tukey tests are two of the several mean separation procedures used in post-ANOVA analysis. The following is the description of how a SNK and a Tukey test can be performed on treatment means:

Student – Newman – Keuls (S-N-K) Procedure:

1) Divide the set of paired comparisons into subsets of order p. The S-N-K procedure has a different critical value for each subset.

2) Specifically, the observed difference of each pair of means in the subset of order p is compared to the critical difference given by

$$SNK(p) = (s_{\bar{d}})r(p,\alpha,v)/\sqrt{2} \qquad (23)$$

For p=1, 2.....7 (for comparing location means) and p=1,2.....10 (for comparing transmissibility means)

Where, $r(p,\alpha,v)$ = studentized range value of order p

v = degrees of freedom on MSE

α = Experimentwise error rate

$(s_{\bar{d}})$ = Standard deviation

3) If the critical difference is less than the difference between 2 means, then those 2 means are said to be significantly different.

Tukey test:

1) The observed difference of any pair of means is compared to the Tukey's critical difference given by

$$TK = (s_{\bar{d}})r(k,\alpha,v)/\sqrt{2} \qquad (24)$$

Where, $r(p,\alpha,v)$ = studentized range value of order p

k = number of means being compared

α = Experimentwise error rate

v = degrees of freedom on MSE

$(s_{\bar{d}})$ = Standard deviation

2) If the critical difference is less than the difference between 2 means, then those 2 means are said to be significantly different.

Table 8 – SNK test for transmissibility means

			α	0.05					
Error	Degrees	of	Freedom	54					
Error	Mean	Square		0.415939					
Number of Means	2	3	4	5	6	7	8	9	10
Critical Range	0.691162	0.830798	0.913830	0.972860	1.018503	1.055623	1.086843	1.113744	1.137348

Grouping	Mean	N	TRANS
	18.1814	7	X3
	17.0300	7	X8
	16.9957	7	X1
	16.9086	7	X2
	16.5871	7	X9
	15.5057	7	X10
	13.8557	7	X5
	12.9543	7	X7
	12.8286	7	X4
	12.0957	7	X6

Table 8 shows the SNK test for transmissibility means and Table 9 shows the SNK test for location means. Table 10 shows the Tukey test for transmissibility means and Table 11 shows Tukey test for location means. The grouping lines indicate the means that are not significantly different. Both the post ANOVA analyses show that the transmissibility

means are more significantly different than the location means. From this we can conclude that the transmissibility of the flow barriers has a larger effect on the simulation responses (in this case bottomhole pressure) as compared to the effect of barrier location.

Table 9 – SNK test for location means

			α	0.05		
Error	Degrees	of	Freedom	54		
Error	Mean	Square		0.415939		
Number of Means	2	3	4	5	6	7
Critical Range	0.578267	0.695096	0.764565	0.813953	0.852141	0.883197
		Grouping	Mean	N	LOCATION	
			15.643	10	7	
			15.534	10	6	
			15.471	10	5	
			15.434	10	4	
			15.343	10	3	
			15.0030	10	2	
			14.632	10	1	

Table 10 – Tukey test for transmissibility means

			α	0.05
Error	Degrees	of	Freedom	54
Error	Mean	Square		0.415939
Critcal	Value of	Studentized	Range	4.66582
Minimum	Significant	Difference		1.1373
	Grouping	Mean	N	Trans
		18.1814	7	X 3
		17.0300	7	X 8
		16.9957	7	X 1
		16.9086	7	X 2
		16.5871	7	X 9
		15.5057	7	X 10
		13.8557	7	X 5
		12.9543	7	X 7
		12.8286	7	X 4
		12.0957	7	X 6

Table 11 – Tukey test for location means

			α	0.05
Error	Degrees	of	Freedom	54
Error	Mean	Square		0.415939
Critcal	Value of	Studentized	Range	4.33055
Minimum	Significant	Difference		0.8832
	Grouping	Mean	N	Loc
		15.6430	10	7
		15.5340	10	6
		15.4710	10	5
		15.4340	10	4
		15.3430	10	3
		15.0030	10	2
		14.6320	10	1

2.2.3 Most Likely Scenario

Taking the drainage volume estimated from the decline type-curve analysis as a control value, the mean of the drainage volumes for the various scenarios are summarized in Table 12. From these tables we conclude that the most likely scenarios of transmissibility multipliers for the two barriers are X4 and X6. For X4, the transmissibility multiplier of the NW barrier is 0.00616 and that of the south barrier is 0.00002. For X6, the transmissibility multiplier of the NW barrier is 0.00119 and that of the south barrier is 0.00006. These results indicate that the NW flow barrier is more leaky compared to the south flow barrier. Under these most likely scenarios of transmissibility multipliers, the south barrier is most likely located at J=24 or J=25, as indicated in Table 13.

We then observe the simulated bottomhole pressure on two scenarios from the experimental design that give a high and a low drainage volume value as compared to that from decline type-curve analysis. The two scenarios are X2 - J=25 (drainage volume is 16.94 MMSTB from Table 6) and X7 - J=22 (drainage volume is 10.81 MMSTB from

Table 6). Fig. 2.9 and Fig. 2.10 show the comparison of simulated bottomhole pressure with the observed bottomhole pressure for these two scenarios. We also perform simulation on the most likely scenario – X6 - J=25 to predict the bottomhole pressure. The result is shown in Fig. 2.11. Overall the match with the field data is pretty good for the most likely scenario as compared to the previous two scenarios, which validates the streamline-based drainage volume calculation approach

Table 12 – Drainage volume means over different transmissibility multipliers

TRANS	N	Mean, MMSTB	Mean-12.43, MMSTB
X1	7	16.99	4.56
X2	7	16.91	4.48
X3	7	18.18	5.75
X4	7	12.83	0.4
X5	7	13.86	1.43
X6	7	12.09	-0.34
X7	7	12.95	0.52
X8	7	17.03	4.6
X9	7	16.59	4.16
X10	7	15.51	3.08

Table 13 – Drainage volume means over different locations for most likely transmissibility multipliers

South Barrier Location	X4	X6
	Drainage Volume, MMSTB	
J=22	11.24	10.57
J=23	11.18	11.03
J = 24	12.89	11.03
J = 25	13.31	12.35
J = 26	13.54	12.99
J = 27	13.71	13.29
J = 28	13.93	13.41

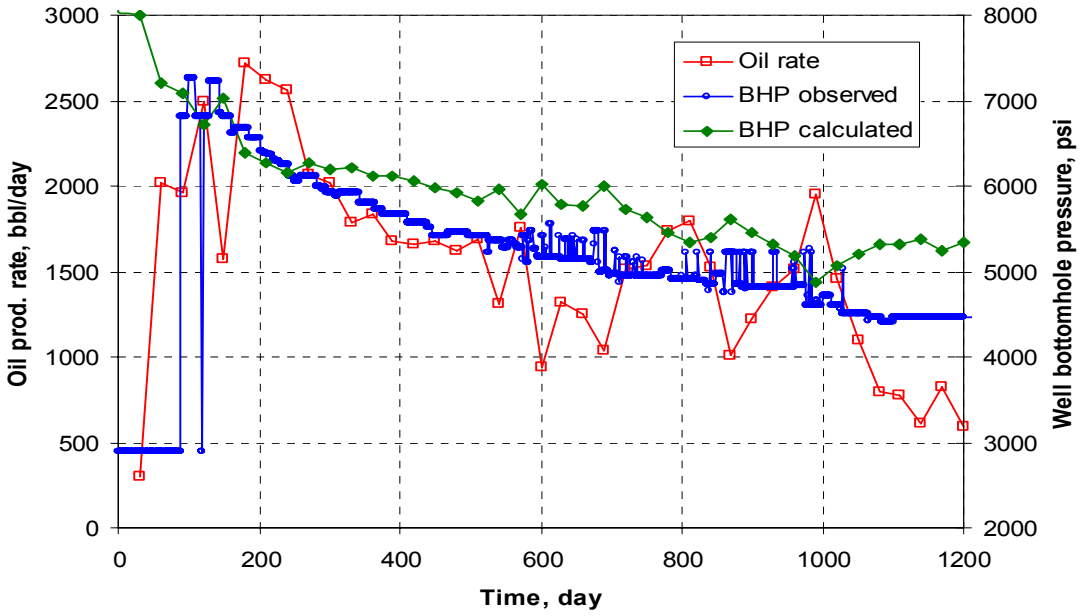

Figure 2.9 – Calculated well bottomhole pressure vs. observed bottomhole pressure for the scenario of X2 and J=25.

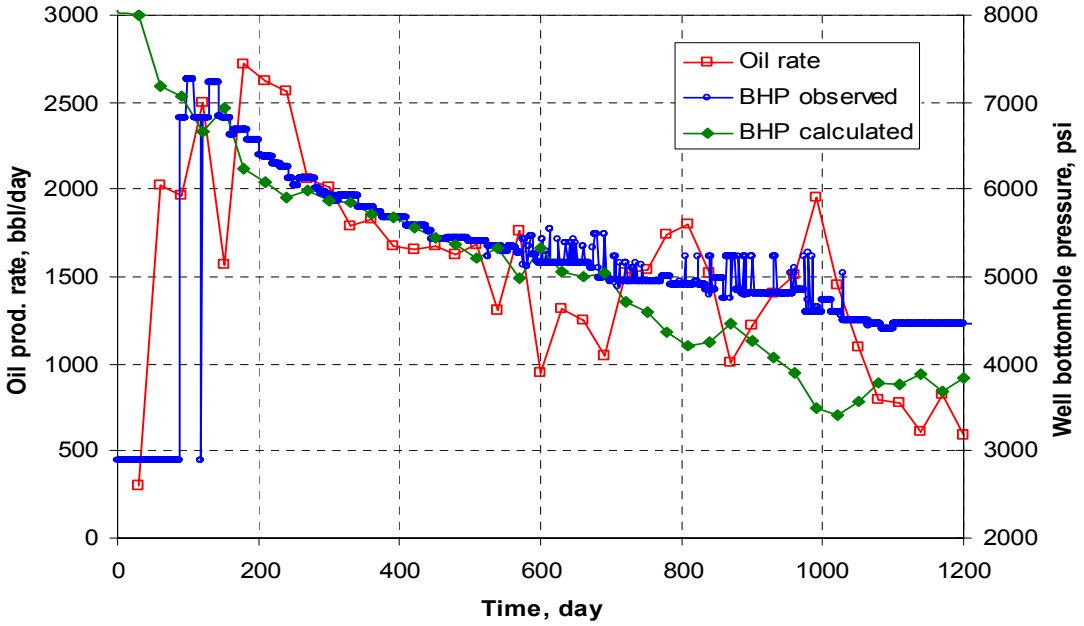

Figure 2.10 – Calculated well bottomhole pressure vs. observed bottomhole pressure for the scenario of X7 and J=22.

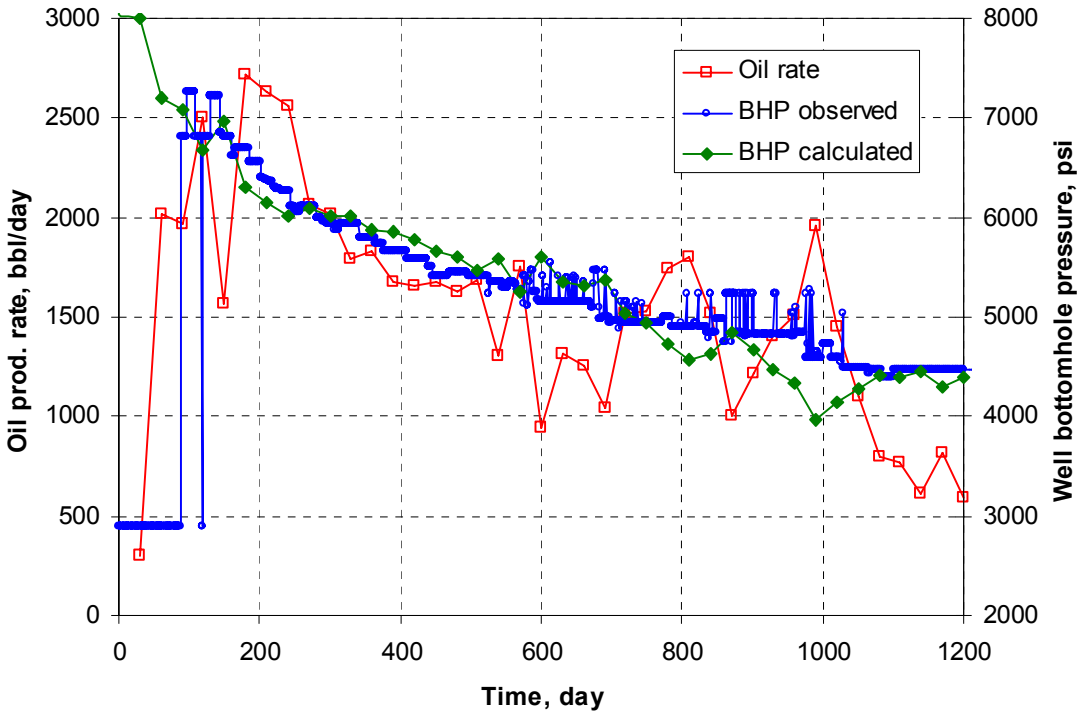

Figure 2.11 – Calculated well bottomhole pressure vs. observed bottomhole pressure for the scenario of X6 and J=25.

2.3 Discussion and Conclusions

From the above discussion it is clear that experimental design and ANOVA acts as an effective tool to quantify the uncertainty in the geologic features of the reservoir simulation model. The experimental design and the LHS approach helps to design a systematic study of the changes in response (drainage volume in our case) with respect to change in the geologic features such as changing transmissibilities and locations of flow barriers. Once we have the drainage volume results in the experimental design, the ANOVA quantifies how much effect each factor has on the drainage volume results. The experimental design analysis also gives the most likely scenario. Performing numerical simulation on this particular scenario, gives a calculated pressure response that agrees well with the observed data.

The following conclusions from this study can be summarized as follows:

1. The transmissibiity of the North west/ South flow barrier has a greater effect on the drainage volume than the location of the south barrier.
2. The Northwest flow barrier is more leaky than the South flow barrier.
3. The most likely position of the South barrier is at J=24 or J=25.
4. The order of magnitude of transmissibility multiplier for south barrier is 10^{-5} and the order of magnitude of transmissibility multiplier for the Northwest barrier is 10^{-3}.

CHAPTER III

IDENTIFICATION OF SIGNIFICANT RESERVOIR MODELING PARAMETERS IN FLOW RESPONSE

The accuracy of flow performance predictions depends on the validity of the reservoir model used for numerical simulation. In real life however, reservoir modeling parameters required to build the reservoir models are highly uncertain. It is therefore necessary to identify significant modeling parameters and study the impact of uncertainty in these modeling parameters on the flow performance. Typically such a study would require a large number of simulation runs, which take too much time. This makes such study unfeasible for quick decision making. We propose to combine a fast approximate simulation technique like streamline simulation with a statistical technique called experimental design and response surface methodology. Experimental Design reduces the number of simulation runs by carefully choosing the combinations of geologic parameters to change. Streamline simulator quantifies the impact on the flow response. In this case, we take the sweep efficiency as the response for waterflooded reservoirs. This particular response variable is very fast to compute with streamline simulation under the steady state pressure conditions we assume.

This chapter would first discuss the theory behind Box-Behnken designs in detail. This is followed by fundamentals of streamline simulation and the method to compute sweep efficiency. The next section discusses the method to identify significant modeling parameters and to quantify the impact of their uncertainty on sweep efficiency in both object and pixel-based modeling methods.

3.1 Box-Behnken Design

Box and Behnken (1960) developed a family of efficient three-level designs for fitting second-order response surfaces. The class of designs is based on the construction of

balanced incomplete block designs. The Box-Behnken design is an efficient option for factors with three evenly spaced levels.

Another important characteristic of the Box-Behnken design is that it is a spherical design. Note, for example, in the Box-Behnken design shown in Fig. 1.1, all of the points are so-called "edge points" (i.e., points that are on the edges of the cube); in this case, all edge points are at a distance $\sqrt{2}$ from the design center. There are no factorial or face points. The Box-Behnken design involves all edge points, but the entire cube is not covered. In fact, there are no points on the corner of the cube or even at a distance $\sqrt{3}$ from the design center. The lack of coverage of the cube should not be viewed as a reason not to use Box-Behnken. It is not meant to be a cuboidal design. However the use of the Box-Behnken should be confined to situations in which one is not interested in predicting response at the extremes, that is, at the corners of the cube. If three levels are required and coverage of the cube is necessary, one should use a face center cube rather than a Box-Behnken design. In our case, we assume that within the parameter range, the most probable values lie near their center values. The extreme values of the parameters are kind of unrealistic and we do not need accurate predictions at extreme values. For that reason, we choose a Box-Behnken design over Face Center Cube.

The spherical nature of the Box-Behnken, combined with the fact that the designs are rotatable or near rotatable, suggests that ample center runs should be used. In our particular case since we have four parameters, use of 3-5 centerpoint or center runs are recommended for Box-Behnken design.

Box-Behnken design is a second-order design. This means that the design results in a second-order polynomial response surface model. The second-order response surface model can be written as follows,

$$\hat{y}_j(\vec{x}) = b_{j,0} + \sum_{i=1}^{k} b_{j,i} x_i + b_{j,k+1} x_1 x_2 + b_{j,k+2} x_1 x_3 + \ldots + b_{j,k(k+1)/2} x_{k-1} x_k + \sum_{i=1}^{k} b_{j,i+k(k+1)/2} x_i^{\,2} \quad (25)$$

where,

y = response variable, subscripts: i= number of coefficient, j= number of response, k = number of parameters, x = parameter value

The column vector of coefficients $\vec{b}$ in the above equation are found by solving:

$$\vec{b} = \{[X^{'}][X]\}^{-1}[X^{'}]\vec{y} \tag{26}$$

where, [X] is a design matrix with the following:

row rank = number of design points

column rank = number of regressors

$\vec{y}$: column vector of observed responses

3.2 Streamline Simulation

The streamline approach provides a unique advantage in computing swept volumes (which is the response parameter in this study) under the most general conditions. The key underlying concept here is the streamline time-of-flight proposed by Datta-Gupta and King.[17] The swept volume being a fundamental quantity is expected to correlate with recovery regardless of the displacement process.

The fundamental quantity in the streamline simulation is the time-of-flight which is simply the travel time of a neutral tracer along the streamlines. The time of flight at a particular gridblock with dimensions x, y and z can be defined as,

$$\tau(x, y, z) = \int \frac{\phi ds}{|\overline{u}|} \tag{27}$$

We can rewrite Eq.27 in a different form as follows

$$\overline{u}.\Delta\tau = \phi \tag{28}$$

The velocity field for a general three-dimensional medium can be expressed in terms of bi-streamfunctions ψ and χ as follows

$$\vec{u} = \nabla\psi \times \nabla\chi \tag{29}$$

A streamline is defined by the intersection of a constant value for ψ with a constant value of χ.

Streamline techniques are based upon a coordinate transformation from the physical space to the time of flight coordinates where all the streamlines can be treated straight lines of varying lengths. This coordinate transformation is greatly facilitated by the fact that the Jacobian of the coordinate transformation assumes an extraordinarily simple form:

$$\left\| \frac{\partial(\tau,\psi,\chi)}{\partial(x,y,z)} \right\| = \nabla\tau.(\nabla\psi \times \nabla\chi) = \nabla\tau.\vec{u} = \phi \tag{30}$$

where we have utilized Eq. 28 and Eq. 29. Thus we have the following relationship between the physical space and the time of flight coordinates following the flow direction,

$$\phi dxdydz = d\tau d\psi d\chi \tag{31}$$

It is now easy to see that the coordinate transformation also preserves pore volume, an essential feature for computing volumetric sweep efficiency.

In three-dimensional flow, we can derive the following expressions for swept volumes:

$$V_{swept}(t) = \iiint \phi dx dy dz \, \theta(t - \tau(x, y, z)) = \iiint d\psi d\chi d\tau \theta(t - \tau(\psi, \chi)) \tag{32}$$

where, θ is the Heaviside function and the integral represents the time of flight that are less than the time of interest. Rather than evaluating such complex integrals in 3-D, the swept volume can be obtained by examining the connectivity in the streamline time-of-flight.

Eq. 32 can be interpreted as simply the connected areas or volumes for a given time-of-flight. Eq. 32 can be approximated as follows

$$V_{swept}(t) = \sum_i \int d\tau(\psi_i) \theta(t - \tau) q(\psi_i) \tag{33}$$

where, θ is the Heaviside function, $q(\psi_i)$ is the volumetric flow rate assigned to the streamline ψ_i and i is the number of streamline.

Consider a 3-D Cartesian array of face connected cells. We can define an indicator variable at each cell based on the time-of-flight. For example, a cell is coded as 'unswept' if the time-of-flight at the analyzed cell is greater than the time of interest and as 'swept' if it is less than or equal to the time of interest. Scanning through the 3-D array and adding the pore volumes of the 'swept' cells we can obtain the swept volume at the time of interest. We can then compute the swept volume efficiency by simply dividing the total pore volume. Also, the accuracy of swept volume calculations will deteriorate if the cell size becomes too large.

From the above discussion, it is clear that the swept volume is a good choice as a measure of reservoir recovery for waterflood operations. It becomes easy to compute this particular response variable quickly for multiple scenarios within the experimental design.

3.3 Object-Based Model

For this particular study, we consider a fluvial reservoir whose characteristic feature is the presence of sinuous sand-filled channels within a background of floodplain shale. From a reservoir modeling perspective, it is convenient to view fluvial reservoirs with a hierarchical classification scheme. This genetic hierarchy of heterogeneities may then be quantitatively modeled by successive coordinate transformations and objects representing lithofacies associations.[36] Permeability models are constructed at the appropriate scale using coordinate systems aligned with depositional continuity. For this study, we will use a GSLIB-style program named FLUVSIM, which is a computer code for such hierarchical object-based modeling, and uses simulated annealing and non-random perturbation rules for conditioning to extensive well data.[37]

Fig. 3.1 illustrates the conceptual model for fluvial facies modeling. There are three facies types, with the geometric specification of each chosen to mimic shapes idealized from observations. The first facies type is background floodplain shale, which is viewed as the matrix within which the reservoir quality or sand objects are embedded. The second facies type is channel sand that fills sinuous abandoned channels. This facies is viewed as the best reservoir quality due to the relatively high energy of deposition and consequent coarser grain size. The sand-filled channels are geometrically defined by a channel width, maximum thickness, and the relative position of the maximum thickness. The third facies type is the levee sand formed along the channel margins. These sands are considered to be poorer quality than the channel fill.

The parameters used to define an abandoned sand-filled channel are illustrated in Figs. 3.2 and 3.3. The channels are defined by an orientation angle, the average departure from the channel direction, the ‘wavelength’ or correlation length of that average departure, thickness, thickness undulation (and correlation length), width/thickness ratio, and width undulation. Each parameter may take a range of possible values according to a triangular probability distribution. The channel center line, width, and thickness are 1-D Gaussian fields along the channel direction coordinate. Fig. 3.4 shows the geometric form adopted for the levee sand. The three distance

parameters (A) lateral extent of the levee, (B) height above the channel datum elevation, (C) depth below the channel datum are used to define the size.

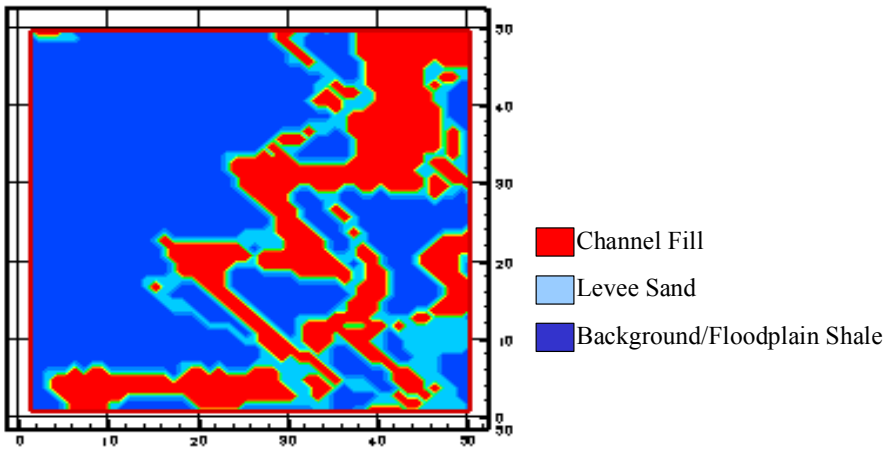

Figure 3.1 – Plan and section view of conceptual model for fluvial facies: background of floodplain shale, sand–filled abandoned channel and levee border sand.

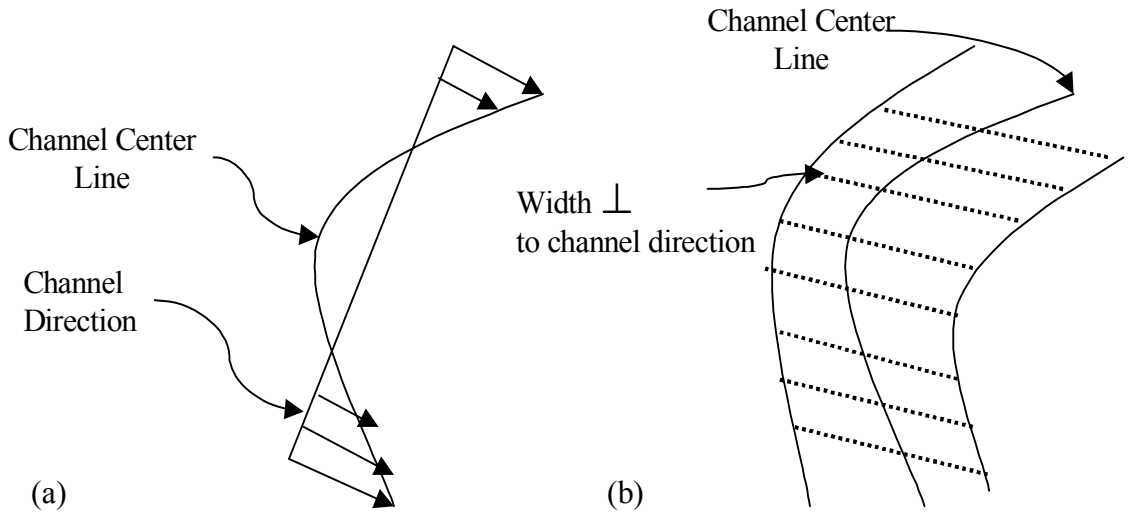

Figure 3.2 – Areal view of some parameters used to define channel object: (a) angle for channel direction and deviation for actual channel center line and (b) variable channel width with connection between channel cross section lines.

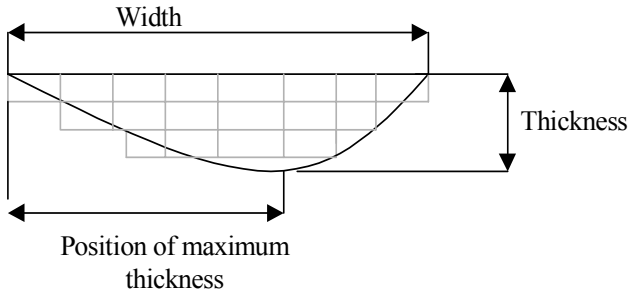

Figure 3.3 – Cross section view of channel object defined by width, thickness, and relative position of maximum thickness.

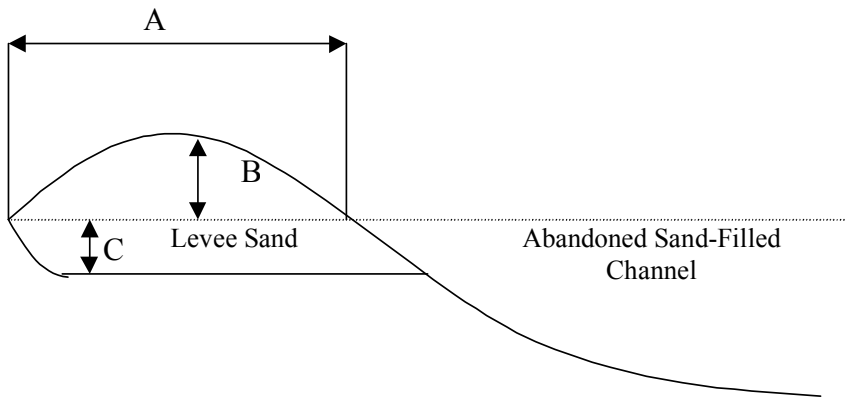

Figure 3.4 – Cross section through abandoned sand-filled channel and levee sand. Three distance parameters (A), (B) and (C) are used to define size of levee sand.

The modeling parameters selected for this study are as follows,

1. Channel Dimensions
   - Thickness
   - Width/Thickness Ratio
2. Sandstone ratio
3. Channel Permeability
   - Channel sand permeability
   - Levee sand permeability

4. Channel Sinuosity

The selection of the modeling parameters is largely subjective. It is important to use a sound judgement while selecting modeling parameters. In this study, we assume the above parameters to be largely uncertain and examine their impact on the flow responses. Table 14 shows the factor ranges. The factor ranges are scaled from –1 to +1. Factor combinations for the simulation models are specified by a 28 experiment Box-Behnken design for the four-factor stochastic model sets. Flow simulation is performed on five realizations at each design point for the stochastic permeability field. The stochasticity in the object-based models comes from the random positioning of the channels.

The synthetic reservoir model for this study (Fig. 3.5) is a 50x50x10-gridblock model with an injector and producer in a Quarter 5-spot pattern. The size of each gridblock is 20x20x10 feet.

Table 15 shows the Box-Behnken experimental design for the object-based reservoir scenarios. The first column indicates the experiment number and the next four columns represent the levels of the four modeling parameters for each experiment. The sixth column represents the mean swept volume efficiencies obtained by performing streamline simulation on five stochastic realizations of each of the 28 scenarios. The seventh column is the standard deviation of the sweep volume for each scenario. The stochastic nature of each scenario is a result of random positioning of channels for a particular scenario in an experiment. Figs. 3.6a, b and c show the permeability, swept volume (at 5000 days) and travel time plot for a particular experiment. This scenario has a high channel dimensions and low channel sinuosity. The travel time plot clearly shows that the high permeability channel zones near the injector are swept almost instantaneously. Similarly we can visualize similar plots for different scenarios to see how our uncertainty in modeling parameters would effect the sweep and travel time plot of the reservoir. Once the flow simulation results for all experiments are obtained we can analyze the design with response surface methodology for identifying significant parameters and for response uncertainty assessment.

Table 14 – Factor Ranges and Scaling for object-based models

		Levels	
Variable	-1	0	1
ChanDim			
thickness (ft)	0.25--1	1--2	2--5
w/t ratio	15--25	25--75	80--100
SandRatio	0.2	0.35	0.5
ChanPet			
Perm (md)	(10,1)	(100,10)	(1000, 100)
Sinuosity (ft)	50	100	150

Table 15 – Experimental design: object-based model

Exp #	ChannelDimen	SandstoneRatio	Petrophysica	Sinuosity	Vol.Sw Eff	Std Deviation
1	0	-1	0	-1	27.18%	8.10%
2	-1	0	0	1	35.48%	3.12%
3	1	0	0	-1	21.57%	8.97%
4	-1	1	0	0	37.01%	3.15%
5	0	1	1	0	43.66%	2.21%
6	0	0	0	0	32.57%	2.04%
7	0	0	0	0	30.59%	2.04%
8	0	0	-1	1	50.65%	0.71%
9	1	0	1	0	25.23%	4.15%
10	-1	0	-1	0	55.05%	1.54%
11	0	0	1	-1	29.12%	1.57%
12	0	1	-1	0	52.59%	0.45%
13	0	0	0	0	32.43%	0.86%
14	-1	0	0	-1	38.22%	0.91%
15	0	1	0	-1	41.58%	1.96%
16	0	0	1	1	28.66%	0.54%
17	0	-1	1	0	11.73%	1.58%
18	1	0	0	1	30.04%	0.27%
19	1	0	-1	0	33.47%	3.24%
20	0	-1	0	1	35.31%	4.47%
21	1	1	0	0	40.16%	1.32%
22	-1	-1	0	0	26.00%	10.83%
23	0	0	0	0	34.62%	0.82%
24	1	-1	0	0	25.41%	1.81%
25	0	1	0	1	44.15%	0.27%
26	0	0	-1	-1	45.67%	3.96%
27	-1	0	1	0	23.38%	1.85%
28	0	-1	-1	0	43.86%	4.41%

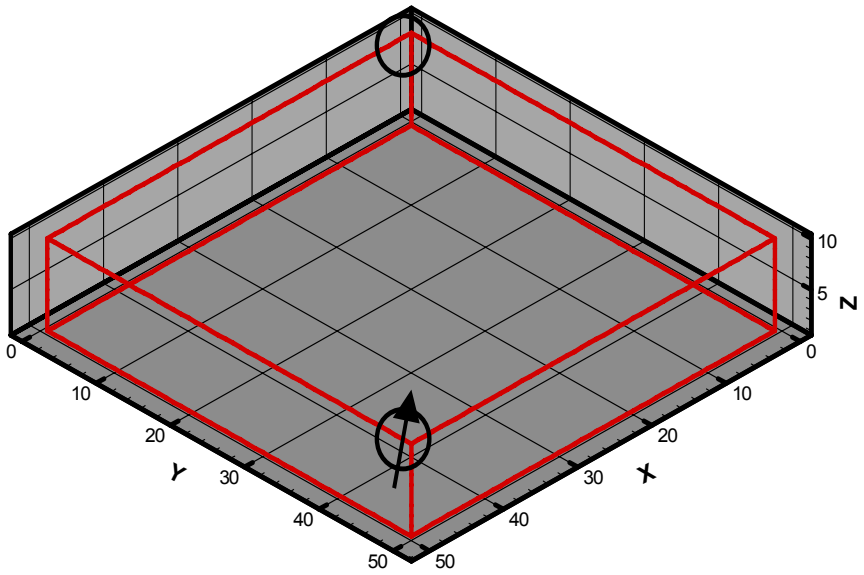

Figure 3.5 – The synthetic reservoir case with an injector-producer in Quarter 5-spot pattern.

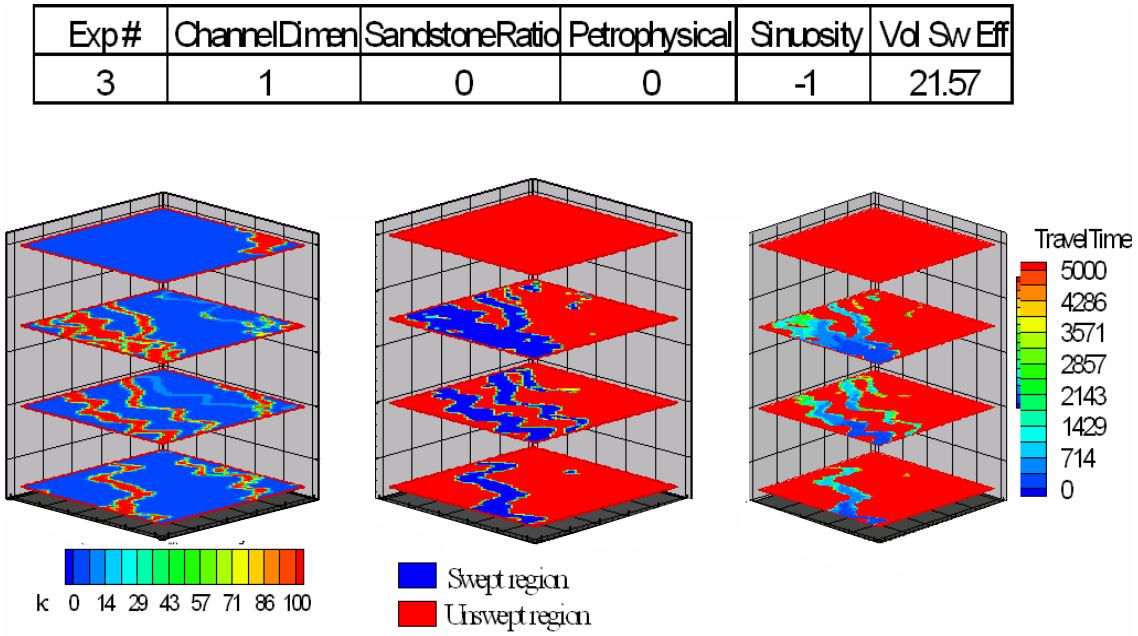

(a) (b) (c)

Figure 3.6 – Plots at a particular experimental design point for object-based models: (a) permeability field, (b) swept region at 5000 days, and (c) travel time plot.

3.3.1 Identification and Uncertainty Analysis

The identification of significant reservoir modeling parameters is achieved by the response surface methodology. The response surface can be directly obtained from the flow responses in the experimental design. In this study, the form of the response surface equation for the object-based model is a function of the modeling parameters.

$$\begin{aligned} SweepEff = {} & b_0 + b_1 \times ChannelDimen + b_2 \times SandstoneRatio + b_3 \times Petroprop \\ & + b_4 \times Sinuosity + b_5 \times (ChannelDimen)^2 + b_6 \times (SandstoneRatio)^2 \\ & + b_7 \times (Petroprop)^2 + b_8 \times (Sinuosity)^2 + b_9 \times ChannelDimen \\ & \times SandstoneRatio + b_{10} \times ChannelDimen \times Petroprop + b_{11} \\ & \times ChannelDimen \times Sinuosity + b_{12} \times SandstoneRatio \times Petroprop \\ & + b_{13} \times Sandstone \times Sinuosity + b_{14} \times Petroprop \times Sinuosity \end{aligned} \tag{34}$$

Table 16 shows the response surface regression results obtained using statistical software called EREGRESS. The first column indicates the coefficient that is computed and the second column shows its value. The third column is the Pr-significant value. The Pr-significant value cut-off for the factor to be significant is chosen as 0.005. This means that the coefficients with Pr-significant value smaller than 0.005 are significant. The fourth column shows the standard error in the estimation of a particular response surface coefficient. The fifth and sixth columns show the –95% and +95% confidence values respectively for a particular response surface coefficient. The highlighted rows show coefficients for parameters that have a significant impact on the flow response. Before using this response surface equation to predict sweep efficiency values over the whole parameter range, we test this response surface model for the experimental design points, for which we have the responses obtained from streamline simulation. Fig. 3.7 shows a plot of predicted sweep efficiency v/s calculated sweep efficiency. The predicted sweep efficiencies are the ones from the response surface model and the calculated sweep efficiencies are the flow simulation results as shown in Table 15. The plot shows a very high correlation coefficient (0.9427) validating the response surface model results.

Table 16 – Response surface coefficients: object-based models

	Coeff value	P value	Std Error	-95%	95%
b0	0.326	8.106e-11	0.01729	0.288	0.363
b1	-0.03271	0.00600	0.00998	-0.05427	-0.01115
b2	0.07472	4.589e-06	0.00998	0.05315	0.09628
b3	-0.09959	1.845e-07	0.00998	-0.121	-0.07803
b4	0.01747	0.104	0.00998	-0.00410	0.03903
b5	-0.02615	0.08675	0.01411	-0.05664	0.00434
b6	0.02089	0.163	0.01411	-0.00960	0.05138
b7	0.03890	0.01635	0.01411	0.00841	0.06939
b8	0.01961	0.188	0.01411	-0.01088	0.05010
b9	0.00934	0.598	0.01729	-0.02801	0.04669
b10	0.05856	0.00486	0.01729	0.02121	0.09591
b11	0.02803	0.129	0.01729	-0.00932	0.06537
b12	0.05801	0.00517	0.01729	0.02066	0.09535
b13	-0.01391	0.436	0.01729	-0.05125	0.02344
b14	-0.01361	0.445	0.01729	-0.05095	0.02374

A plot of residuals (difference between calculated and predicted sweep volume) v/s the predicted sweep volume (Fig. 3.8) shows that the residual values are of the order of magnitude of 10^{-2}. This allows us to further use the response surface as a predictive tool to obtain flow responses over the whole parameter uncertainty range. Figs. 3.9 a, b, c, d, e, f and g show the response surface over the uncertainty range of different modeling parameters. The response surface can then be utilized to predict the scenarios for which we have high and low values of sweep efficiency. Table 17 shows the scenarios predicted to have the best and worst sweep efficiencies and Figs. 3.10 a and b show the corresponding permeability fields, sweep volumes and time-of-flight plots for the two scenarios. The best-case scenario (Table 17) has a very high sandstone ratio, very low channel dimensions and high channel sinuosity. Hence we see a large number of small channels covering all the areas of the reservoir (Fig. 3.10 a). Also the permeability contrast between sandstone and shale is low for the best-case scenario. All these parameter combination lead to high sweep efficiency (56.7%). On the other hand, the worst-case scenario (Table 17) has high channel dimensions, low sandstone ratio and low channel sinuosity. This results in less number of channels covering only some areas of the reservoir (Fig. 3.10 b). The high permeability contrast between sandstone and

shale further reduce the sweep volume. All these parameter combination lead to low sweep efficiency (11.2%).

Table 17 – Scenarios with highest and lowest sweep efficiency in object-based models

	Parameters				
Scenario	ChanDim	PetroPhy	SandRatio	Sinuosity	Sweep Eff %
Best	-1	-1	1	1	56.7
Worst	1	1	-1	-1	11.2

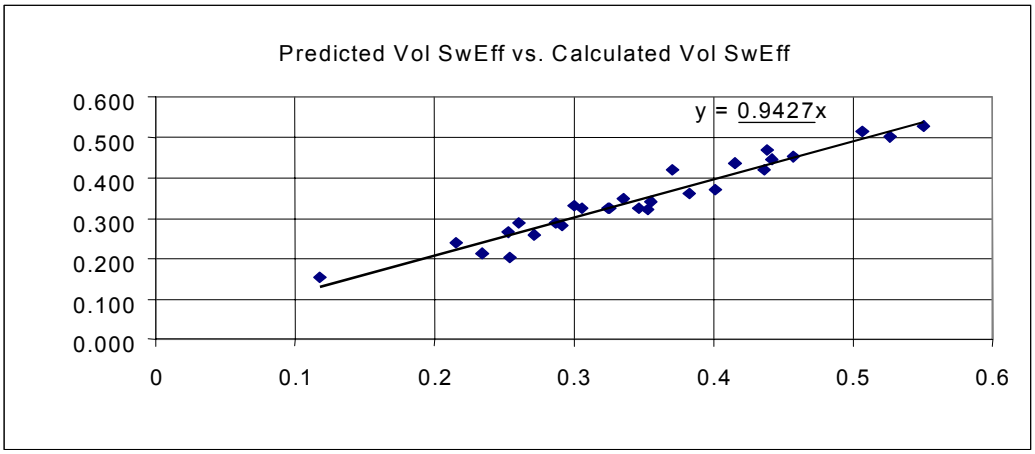

Figure 3.7 – Response surface validation for object-based modeling parameters.

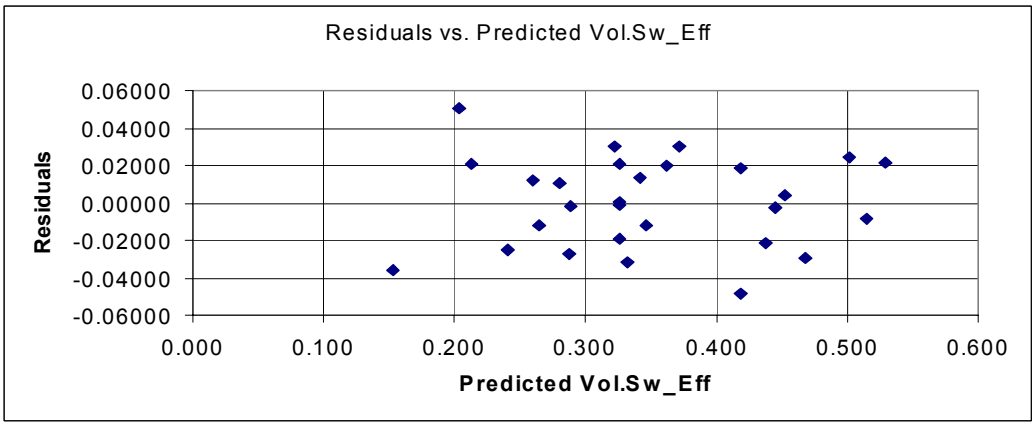

Figure 3.8 – Residuals v/s predicted sweep volume for object-based models.

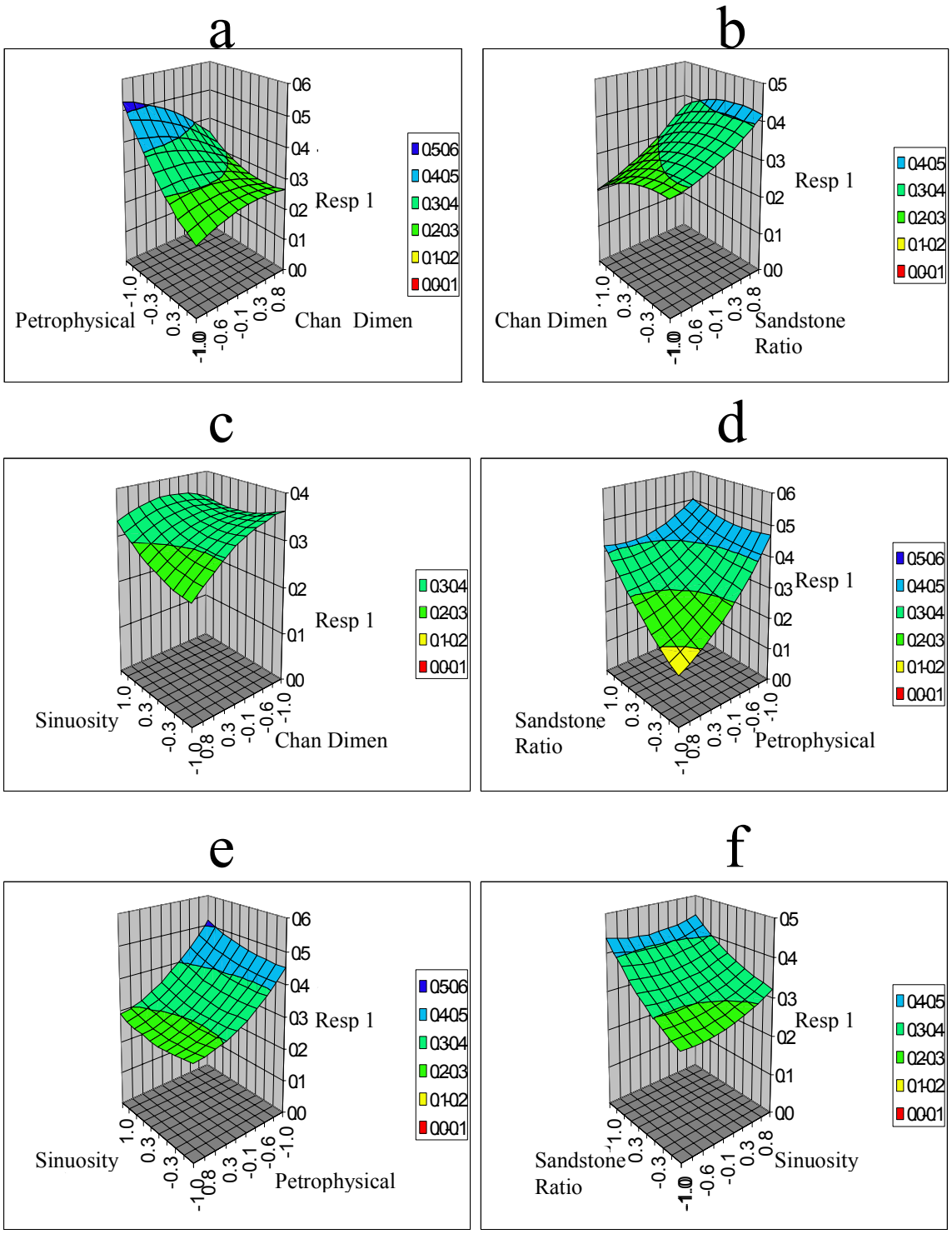

Figure 3.9 – Response surfaces over the uncertainty range of object-based modeling parameters.

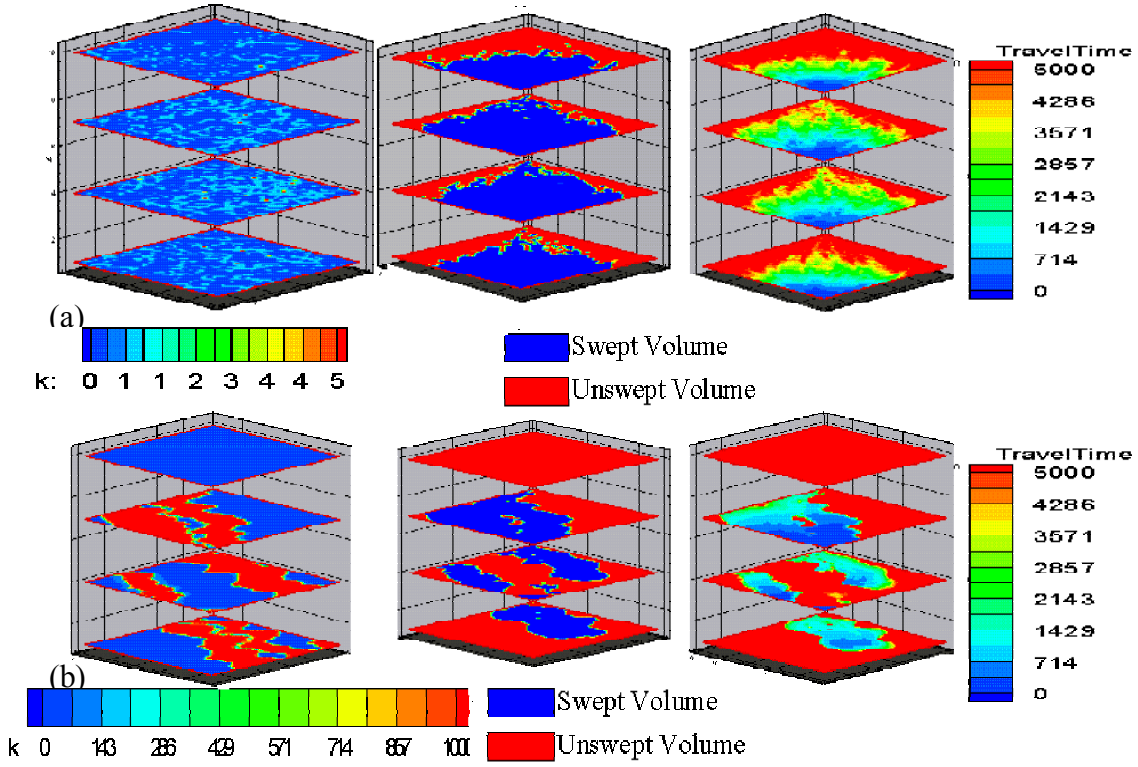

Figure 3.10 – Scenarios predicted by response surface in object-based models to give (a) best sweep efficiency, and (b) worst sweep efficiency.

3.3.2 Results and Conclusions

From Table 16 and Fig. 3.9 we can conclude that the following uncertain modeling parameters have a significant impact on the flow response:

- Petrophysical properties (channel and levee sand permeabilities)
- Sandstone Ratio
- Interaction parameter of channel dimensions and petrophysical properties
- Interaction parameter of sandstone ratio and petrophysical properties.

The petrophysical properties have the largest impact on the flow responses. Figs. 3.7 and 3.8 also indicate that we can use the response surface as a tool to predict flow responses without spending resources on numerical simulation in object-based models. Also, the

response surfaces in Fig. 3.9 provide quick insights into flow response-parameter relationships. It is also clear that the uncertainty in certain object-based modeling parameters has a large impact on the flow responses. The response surface can predict the scenarios for which we get the best and the worst flow response.

3.4 Pixel-Based Model

A similar synthetic fluvial reservoir which we modeled using object-based modeling technique is now modeled using a pixel-based technique. We use sequential indicator simulation (SIS) which is a pixel-based simulation algorithm that builds a categorical image, pixel by pixel, by drawing from a non-parametric conditional distribution. Unlike object-based models, for pixel-based algorithms, the resulting geometries (for each category) tend to be noisy. However, conditioning to well data is not a problem in pixel-based methods like SIS. We use an indicator simulation with three categories since we have three facies similar to the ones in the reservoir model used in object-based technique. For this particular study, we use the GSLIB sisim program.

For the single multiple indicator simulation the following sequence is adopted. The indicator is defined by three categories, each category representing a particular facies. Also the well data is represented as indicator data for each layer in the reservoir model. We carry out a sequence of indicator krigings at each node, conditional to neighboring well indicator data and previously simulated indicator values. This indicator kriging requires the 3D variogram of the indicator variable. The parameters used to model this indicator variogram (range, sill and nugget) can be highly uncertain. Geological interpretation of the channel sizes usually helps us in evaluating the uncertainty of the variogram range. The sum of sill and nugget is set to 1 and both the sill and nugget are varied accordingly to study their impact on flow responses.

The modeling parameters selected for this study are as follows,

1. Variogram Range
   - Major Axis
   - Minor Axis

2. Sandstone ratio
3. Channel Permeability
   - Channel sand permeability
   - Levee sand permeability
4. Variogram Parameters
   - Nugget
   - Sill

The sandstone ratio is changed by changing the sandstone pdf cut off value, which indicates the probability of sandstone facies in the reservoir model. The channel and levee sand permeability range is the same as that in object-based models.

Table 18 shows the factor ranges. The factor ranges are scaled from –1 to +1. Factor combinations for the simulation models are specified by a 28 experiment Box-Behnken design for the four-factor stochastic model sets. Five realizations are run at each design point for the stochastic permeability field.

The synthetic reservoir model for this study is a 50x50x10-gridblock model with an injector and producer in a Quarter 5-spot pattern. The size of each gridblock is 20x20x10 feet. This reservoir is the same as used in object-based modeling.

Table 19 shows the Box-Behnken experimental design for the object-based reservoir scenarios. The first column indicates the experiment number and the next four columns represent the levels of the four modeling parameters for each experiment. The sixth column represents the mean sweep volume efficiencies obtained by performing streamline simulation on five stochastic realizations of each of the 28 scenarios. The seventh column is the standard deviation of the sweep volume for each scenario.

Figs. 3.11 a, b and c show the permeability, swept volume (at 5000 days) and travel time plot for a particular experiment. This scenario has a high variogram range and low sandstone ratio. The travel time plot clearly shows that the high permeability channel zones near the injector are swept almost instantaneously. Similarly we can visualize similar plots for different scenarios to see how our uncertainty in modeling parameters would affect the sweep and travel time plot of the reservoir. Once the flow simulation

results for all experiments are obtained we can analyze the design with response surface methodology for identifying significant parameters and for response uncertainty assessment.

Table 18 – Factor ranges and scaling for pixel-based models

Parameter	-1	0	1
Variogram Range			
a_hmax	100.00	500.00	1000.00
a_hmin	10.00	50.00	100.00
Sanstone pdf cut-off	0.2	0.35	0.5
ChanPet			
Perm	(10,1)	(100,10)	(1000, 100)
Variogram			
nugget	0	0.4	0.8
sill	1	0.6	0.2

Table 19 – Experimental design: pixel-based model

Exp #	Variogramrange	pdfcutoff	petrophysical	Nugget&Sill	Vol Sw.Eff	Std Deviation
1	1	-1	0	0	24.01%	0.78%
2	-1	0	-1	0	53.34%	1.27%
3	0	0	-1	1	51.93%	0.67%
4	0	1	1	0	44.56%	1.88%
5	0	0	1	-1	10.57%	1.86%
6	-1	0	0	1	31.01%	5.04%
7	1	0	0	1	35.36%	0.79%
8	0	0	0	0	30.94%	2.08%
9	0	0	0	0	30.29%	2.41%
10	0	1	-1	0	50.53%	0.64%
11	0	0	0	0	30.71%	2.64%
12	0	0	1	1	12.56%	3.52%
13	-1	0	0	-1	28.03%	4.84%
14	1	0	-1	0	47.62%	1.06%
15	1	0	1	0	17.42%	3.47%
16	0	-1	-1	0	58.95%	0.76%
17	-1	1	0	0	47.57%	0.34%
18	0	-1	0	1	24.86%	3.04%
19	-1	-1	0	0	25.13%	1.80%
20	0	0	0	0	30.33%	1.72%
21	0	-1	1	0	9.93%	1.68%
22	0	-1	0	-1	12.98%	1.32%
23	0	1	0	1	46.25%	5.36%
24	0	1	0	-1	34.87%	1.23%
25	0	0	-1	-1	40.62%	3.83%
26	-1	0	1	0	24.77%	0.62%
27	1	1	0	0	45.60%	0.53%
28	1	0	0	-1	11.41%	1.17%

Exp #	VariogramRange	pdf cutoff	Petrophysical	Nugget&Sill	Vol Sw Eff
1	1	-1	0	0	24.01

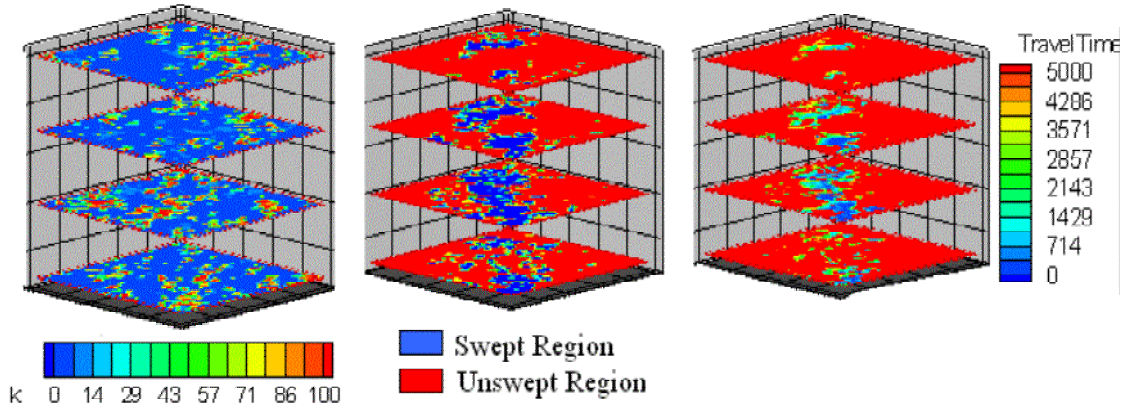

(a) (b) (c)

Figure 3.11 – Plots at a particular experimental design point in pixel-based models: (a) permeability field, (b) swept region at 5000 days, and (c) travel time plot.

3.4.1 Identification and Uncertainty Analysis

The identification of significant reservoir modeling parameters is achieved by the response surface methodology. The response surface can be directly obtained from the flow responses in the experimental design. In this study, the form of the response surface equation for the pixel-based model is a function of the modeling parameters.

$$\begin{aligned} SweepEff = {} & b_0 + b_1 \times VarioRange + b_2 \times SandstoneRatio + b_3 \times Petroprop \\ & + b_4 \times Nugget + b_5 \times (VarioRange)^2 + b_6 \times (SandstoneRatio)^2 \\ & + b_7 \times (Petroprop)^2 + b_8 \times (Nugget)^2 + b_9 \times VarioRange \\ & \times SandstoneRatio + b_{10} \times VarioRange \times Petroprop + b_{11} \\ & \times VarioRange \times Nugget + b_{12} \times SandstoneRatio \times Petroprop \\ & + b_{13} \times Sandstone \times Nugget + b_{14} \times Petroprop \times Nugget \end{aligned} \tag{35}$$

Table 20 shows the response surface regression results obtained using a statistical software called EREGRESS. The first column indicates the coefficient that is computed and the second column shows its value. The third column is the Pr-significant value. The Pr-significant value cut-off for the factor to be significant is chosen as 0.005. This means that the coefficients with Pr-significant value smaller than 0.005 are significant. The fourth column shows the standard error in the estimation of a particular response surface coefficient. The fifth and sixth columns show the –95% and +95% confidence values respectively for a particular response surface coefficient. The highlighted rows show coefficients for parameters that have a significant impact on the flow response. Before using this response surface equation to predict sweep efficiency values over the whole parameter range, we test this response surface model for the experimental design points, for which we have the responses obtained from streamline simulation. Fig. 3.12 shows a plot of predicted sweep efficiency v/s calculated sweep efficiency. The predicted sweep efficiencies are the ones from the response surface model and the calculated sweep efficiencies are the flow simulation results as shown in Table 19. The plot shows a very high correlation coefficient (0.9771) validating the response surface model results. A plot of residuals (difference between calculated and predicted sweep volume) v/s the predicted sweep volume (Fig. 3.13) shows that the residual values are of the order of magnitude of 10^{-2}. This allows us to further use the response surface as a predictive tool to obtain flow responses over the whole parameter uncertainty range. This allows us to further use the response surface as a predictive tool to obtain flow responses over the whole parameter uncertainty range. Figs. 3.14. a, b, c, d, e, f and g show the response surface over the uncertainty range of different modeling parameters.

The response surface can then be utilized to predict the scenarios for which we have high and low values of sweep efficiency. Table 21 shows the scenarios predicted to have the best and worst sweep efficiencies and Figs. 3.15 a and b show the corresponding permeability fields, sweep volume and time-of-flight plot for the two scenarios. The best case scenario (Table 21) has a very high sandstone ratio and very high variogram range. Since the variogram range is directly proportional to the length of the channel, we see a

large number of continuous channels covering all the areas of the reservoir (Fig. 3.15 a). Also the permeability contrast between sandstone and shale is low for the best-case scenario. All these parameter combination lead to high sweep efficiency (59.78%). On the other hand, the worst-case scenario (Table 21) has low variogram range and low sandstone ratio. This results in less number of channels covering only some areas of the reservoir (Fig. 3.15 b). The high permeability contrast between sandstone and shale further reduce the sweep volume. All these parameter combination lead to low sweep efficiency (0.1763%). A high nugget setting for both the scenarios indicates a pure nugget effect. For best-case scenario, the pure nugget effect results in a large number of continuous channel networks throughout the reservoir due to its large variogram range and high sandstone ratio. This leads to a high swept volume. For the worst-case scenario, the pure nugget effect results in a small number of discontinuous channels throughout the reservoir due to its small variogram range and low sandstone ratio. This leads to a low swept volume.

Table 20 – Response surface coefficients: pixel-based models

	coeff value	P value	Std Error	-95%	95%
b0	0.306	5.345e-11	0.01570	0.272	0.340
b1	-0.02369	0.02148	0.00907	-0.04327	-0.00410
b2	0.09459	1.098e-07	0.00907	0.07500	0.114
b3	-0.153	3.297e-10	0.00907	-0.172	-0.133
b4	0.05292	5.808e-05	0.00907	0.03334	0.07251
b5	0.00713	0.588	0.01282	-0.02057	0.03483
b6	0.04958	0.00194	0.01282	0.02188	0.07728
b7	0.04655	0.00305	0.01282	0.01885	0.07425
b8	-0.05640	0.000719	0.01282	-0.08410	-0.02870
b9	-0.00211	0.895	0.01570	-0.03604	0.03181
b10	-0.00407	0.800	0.01570	-0.03799	0.02986
b11	0.05245	0.00533	0.01570	0.01852	0.08637
b12	0.108	1.163e-05	0.01570	0.07371	0.142
b13	-0.00126	0.937	0.01570	-0.03519	0.03266
b14	-0.02330	0.162	0.01570	-0.05722	0.01063

Table 21 – Scenarios with highest and lowest sweep efficiency in pixel-based models

	Parameters				
Scenario	Nugget	VarioRange	SandRatio	Petrophy	Sweep Eff %
Best	1	1	1	-1	59.78
Worst	1	-1	-1	1	0.1763

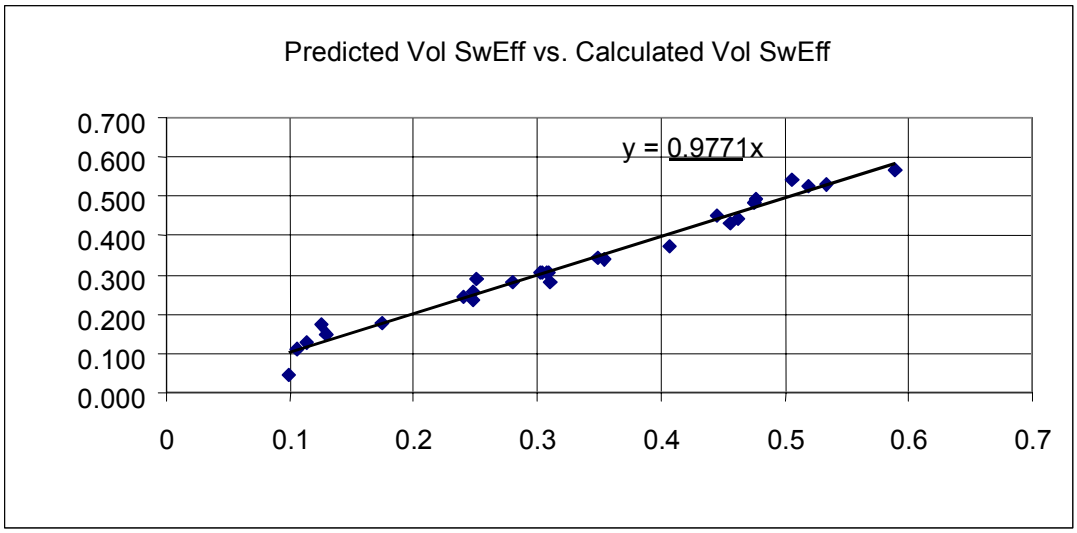

Figure 3.12 – Response surface validation for pixel-based modeling parameters.

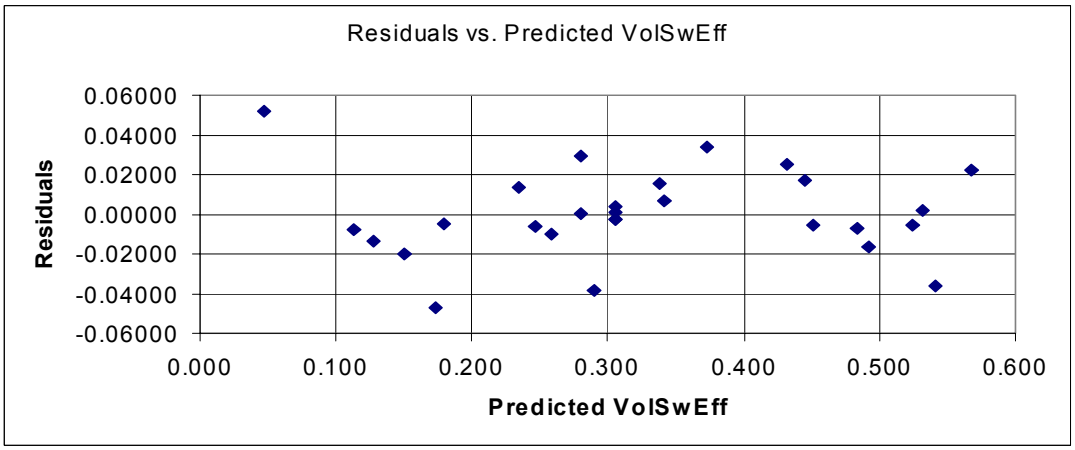

Figure 3.13 – Residuals vs. predicted sweep efficiency for pixel-based models.

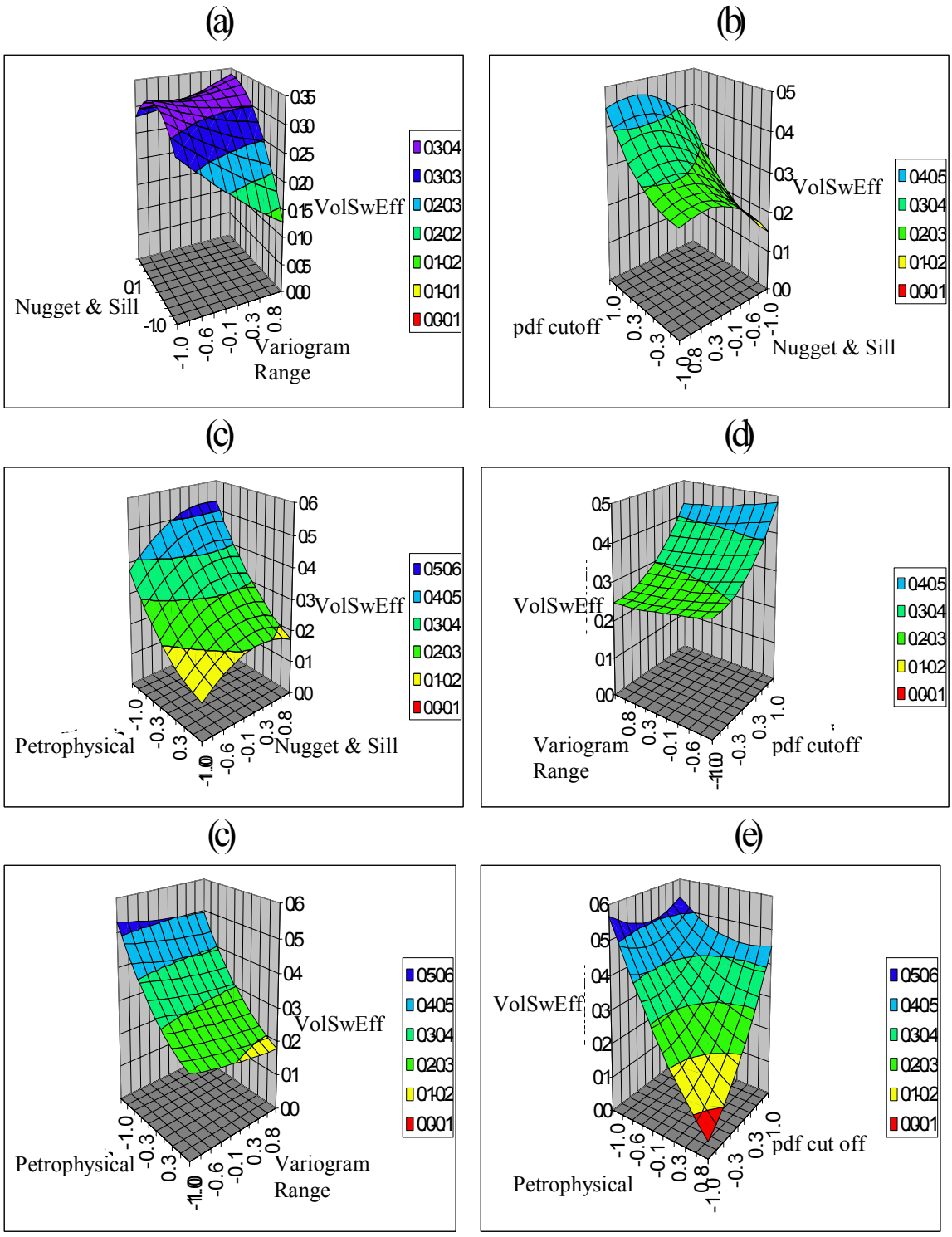

Figure 3.14 – Response surfaces over the uncertainty range of pixel-based modeling parameters.

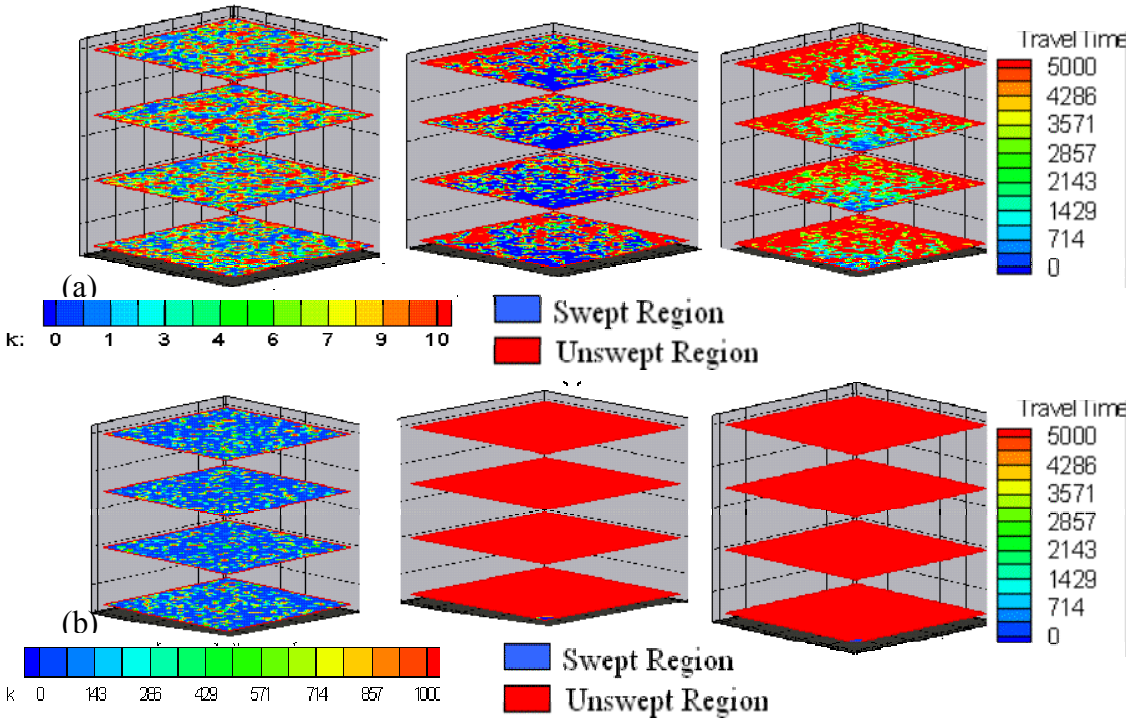

Figure 3.15 – Scenarios predicted by response surface in pixel-based models to give (a) best sweep efficiency, and (b) worst sweep efficiency.

3.4.2 Results and Conclusions

From Table 20 and Fig. 3.14 we can conclude that the following uncertain modeling parameters have a significant impact on the flow response:

- Petrophysical properties (channel and levee sand permeabilities)
- Sandstone Ratio
- Variogram nugget
- Quadratic Parameters of the petrophysical properties, sandstone ratio and Variogram Nugget
- Interaction parameter of sandstone ratio and petrophysical properties.

As in the object-based models, the petrophysical properties have the largest impact on the flow responses. Figs.3.12 and 3.13 also indicate that we can use the response surface as a tool to predict flow responses without spending resources on numerical simulation

in pixel-based models. Also, the response surfaces in Fig. 3.14 provide quick insights into flow response-parameter relationships. It is also clear that the uncertainty in certain pixel-based modeling parameters has a large impact on the flow responses. The response surface can predict the scenarios for which we get the best and the worst flow response.

3.5 Discussion

It is interesting to compare the results from the object-based and pixel-based models. The overall mean swept volume efficiency in both the modeling techniques are approximately the same. For object-based modeling technique the overall mean (b_0) is 32.6% (Table 16). For pixel-based modeling technique the overall mean (b_0) is 30.6% (Table 20). Also, the sandstone channel permeability is the most significant parameter in both the modeling techniques since it has the largest impact on flow responses in both the modeling techniques.

We can derive a physical meaning by checking the response surface behavior over individual parameters. For example in Fig. 3.14c, the response first increases with an increase in the nugget value (and a variable channel permeability value) and then decreases as the nugget value approaches 1. This is because at a low nugget value, the variogram is stable resulting in the channels to be continuous. This results in lower sweep efficiency. As the nugget value increases, the channels become more discontinuous which results in minimum preferential flow. Hence we would then observe higher sweep volume. However at nugget values approximately greater than 0.4 (rescaled value), the channels become highly discontinuous. This results in a loss in connectivity of the high permeability channels leading to a lower swept volume.

Increasing the sandstone permeability increases the permeability contrast with the permeability of the surrounding shale matrix (which we assume to be constant), resulting in all the injected water flowing through the high permeability sandstone channels. This would then result in low sweep efficiency. Lower sandstone channel permeability decreases the permeability contrast, which then results in an increase in swept volume. This feature is captured by the response surface.

The significance of interaction parameters, especially between sandstone ratio and petrophysical properties, on flow responses indicates that flow behavior would change with respect to sandstone ratio if the petrophysical properties are changed and vice-versa. Another important significant interaction parameter is between channel dimensions and petrophysical properties.

Another important aspect of this study is that we performed quick streamline simulation on five different realizations within each scenario for both object and pixel-based models. In theory, we can have infinite number of stochastic realizations. It is then interesting to see the response surface of the variance of flow responses within each scenario for object-based models. The variance in object-based model is due to its stochastic nature, which comes from the random positioning of the channels for different random numbers within a scenario. The variance for each scenario represents the stochastic nature for that particular set of parameter values. Figs. 3.16. a, b, c, d, e and f show the response surfaces for variance in swept volume with respect to the object-based modeling parameters. This figure then gives a useful insight as to how the uncertainty in modeling parameters affects the stochastic nature of the object-based modeling technique. This exercise would be extremely useful to rank stochastic object-based reservoir models that also have uncertain modeling parameter ranges. The response surface can be optimized to get the modeling parameter values at which the variance due to stochastic nature is the minimum. Hence, for object based models, we can have parameter values at which the flow response is the best and worst (Table 17 and Fig. 3.10) and the parameter values at which the variance or standard deviation in sweep volume due to stochastic nature is minimum and maximum (Table 22 and Figs. 3.17 a and b). Figs. 3.17 a and b represent the permeability plots of scenarios with minimum and maximum sweep volume variance respectively. Fig. 3.17 a. clearly shows a large number of low sinuosity channels running through the whole reservoir. Since the variance in swept volume comes from the random positioning of the channels, the variance in swept volume for this permeability scenario would be negligible. Fig. 3.17 b. shows very few low sinuosity channels running through the reservoir. This indicates that

the swept volume would largely depend on where these channels are positioned. Hence we observe a large variance in swept volume for this permeability scenario. Flow response in the scenario, with minimum sweep efficiency variance, is least affected by the random positioning of the channels. Flow response in the scenario, with maximum sweep efficiency variance, is largely affected by the random positioning of the channels.

The following general conclusions can be drawn from this study:

1. Experimental Design/Response surface methodology can be integrated with reservoir modeling techniques for studying the impact of uncertain modeling parameters on reservoir flow response.
2. Response Surfaces can be used to predict simplified flow responses without spending resources for numerical simulation, particularly for ranking and prioritization of model parameters
3. A fast flow modeling technique like streamline simulation combined with a statistical technique like experimental design can provide quick insights for response-parameter relationships.
4. The impact of the uncertainty in modeling parameters on the stochastic nature of the object-based modeling technique can be studied.

Table 22 – Scenarios with minimum and maximum variances in object-based models

	Parameters				
Scenario	ChanDim	Petrophy	SandRatio	Sinuosity	Standard Deviation
Minimum Sweep Variance	-1	-1	1	-1	0%
Maximum Sweep Variance	-1	-0.75	-1	-1	12%

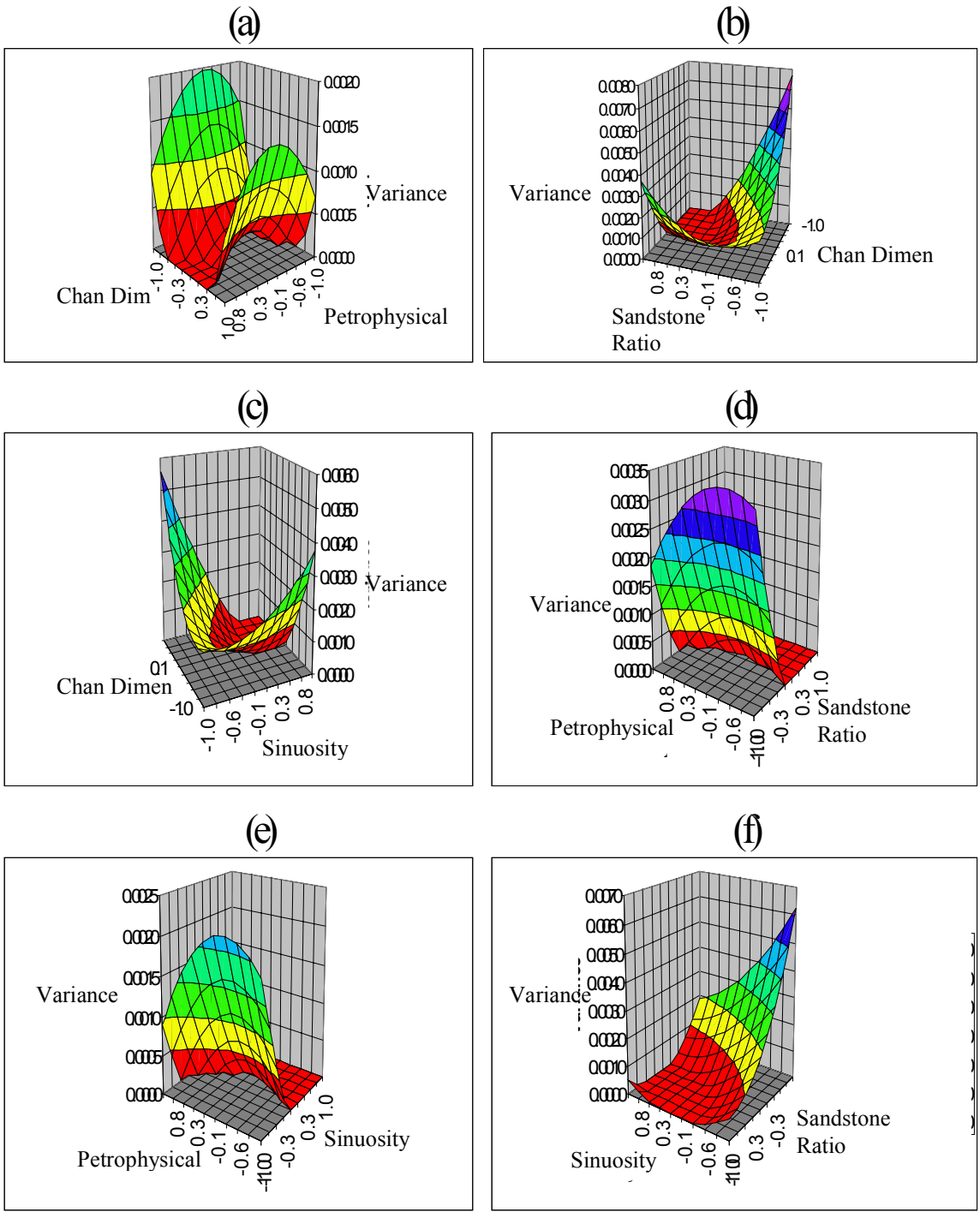

Figure 3.16 – Response surfaces of sweep volume variances over the uncertainty range of modeling parameters in object-based models.

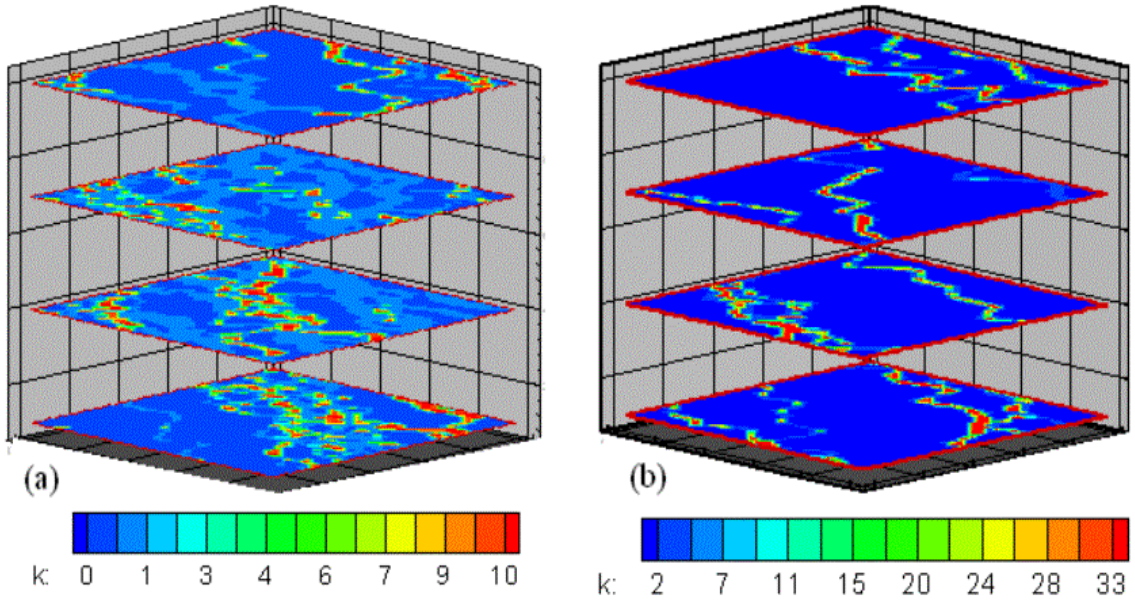

Figure 3.17 – Scenarios predicted by response surface of variances in sweep volume for object-based models to give (a) minimum sweep efficiency variance, and (b) maximum sweep efficiency variance.

CHAPTER IV

CONCLUSIONS AND FUTURE WORK

This research successfully applied a statistical tool called experimental design and response surface methodology for a reservoir characterization problem and for flow uncertainty assessment.

In the first study, the drainage volumes, obtained from decline curve analysis and 'diffusive' time-of-flight concept, are matched via experimental design leading to two conclusions which can be used for similar kind of studies:

- Experimental design can be successfully used to characterize barrier locations and barrier transmissibility in different reservoirs
- The 'diffusive' time-of-flight approach to calculate drainage volume is further validated by the experimental design.

Streamline-based drainage volume calculations in conjunction with conventional decline type curve analysis can provide a powerful approach to identification of reservoir compartmentalization and flow barriers during early stages of reservoir development. This approach relies on inferring flow barriers and reservoir compartmentalization based on a drainage volume matching. Thus, the results will be non-unique in general and will require prior geologic knowledge or additional information to address such non-uniqueness. The experimental design and Analysis of Variance quantifies this uncertainty in the location and strength of the flow barriers

The second study successfully integrates experimental design/response surface methodology with reservoir modeling and flow simulation to study the impact of uncertain modeling parameters on the reservoir flow response. First, the study reveals the modeling parameters that significantly affect flow response. The response surface analysis then tells us how exactly the flow response behaves within the uncertainty range of modeling parameters. Further study to optimize the response surface for the minimum and maximum flow response, reveals the worst reservoir model and the best reservoir

model scenarios in terms of flow response. The worst reservoir model can be considered as a pessimistic case for recovery predictions and the best reservoir model can be considered as the optimistic case for the recovery predictions. Hence, one can obtain a preliminary ranking of reservoir models based on the uncertainty in model parameters. For the object-based models, we also analyze the response surface of the flow response variance. This analysis gives us the scenarios that would show maximum and minimum variability of flow response due to the random positioning of the high-permeability channels. The above two analysis combined would then help us to identify scenarios where the flow response might be favorable but also might be highly uncertain and largely dependent on the positioning of channels. It could also help us identify scenarios with a highly predictable flow response.

The future work would involve successful application of the experimental design/response surface procedure on a field case. It would be interesting to see if the response surface can predict the flow responses accurately for a complicated field case. Another area of research would be the application of response surface methodology for history matching purposes. Response surfaces can be used to compute sensitivities or flow responses instead of the flow simulator, which can significantly reduce the computation time for history matching large reservoirs.

NOMENCLATURE

DF	=degrees of freedom
F	=test statistic
MSError	= experimental error mean squares
MSLoc	= location mean squares
MSTrans	= transmissibility mean squares
P	=significance level
SSError	= experimental error sum of squares
SSLoc	= location sum of squares
SSTrans	= transmissibility sum of squares
SSY	= total sum of squares
A	=drainage area
B_o	=formation factor of oil
C_a	=shape factor of drainage area
c_e	=effective compressibility
c_f	=rock compressibility
c_o	=oil compressibility
c_w	=water compressibility
c_t	=total compressbility
h	=formation thickeness
K	=permeability of reservoir
K_o	=effective permeability of oil
N_p	=cumulative production of well
p_i	=initial reservoir pressure
p_{wf}	=flow bottomhole pressure of well
q	=production rate of well
q_{Dd}	=dimensionless production rate
r_D	=dimensionless radius

r_w'	=effecitive wellbore radius
s	=distance along streamline
S_o	=oil saturation
S_w	=water saturation
t_D	=dimensionless time
$\bar{t}$	=material balance time
$\bar{t}_{Dd}$	=dimensionless material balance time
ϕ	=porosity
γ	=Euler constant
λ_t	=total mobility
μ_o	=viscosity of oil
τ	=time of flight
τ'	='Diffusive' time of flight
θ	=Heaviside function
ψ, χ	=bi-streamfunctions

REFERENCES

1. White, C.D., Willis, B.J., Narayanan, K. and Dutton, S.P.: "Identifying and Estimating Significant Geologic Parameters With Experimental Design," *SPEJ*, (Sept 2001), 311-324.
2. Brandsaeter, I., Wist, H.T., Naess, A., Lia, O., Arntzen, J. *et al*.: "Ranking of Stochastic Realizations of Complex Tidal Reservoirs Using Streamline Simulation Criteria," *Petroleum Geoscience* (2001) **7**, S53-S63.
3. Manceau, E., Mezghani, M., Zabala-Mezghani, I. and Roggero, F.: "Combination of Experimental Design and Joint Modeling Methods for Quantifying the Risk Associated With Deterministic and Stochastic Uncertainties-An Integrated Test Study," paper SPE 71620 presented at the 2001 SPE Annual Technical Conference and Exhibition, New Orleans, Louisiana, September 30-October 3.
4. Friedmann, F., Chawathe, A. and Larue, D.K.: "Assessing Uncertainty in Channelized Reservoirs Using Experimental Designs," paper SPE 71622 presented at the 2001 SPE Annual Technical Conference and Exhibition, New Orleans, Louisiana, September 30-October 3.
5. White, C.D. and Royer, S.A.: "Experimental Design as a Framework for Reservoir Studies," paper SPE 79676 presented at the 2003 SPE Reservoir Simulation Symposium, Houston, Texas, February 3-5.
6. Parish, R.G., Calderbank, V.J., Watkins, A.J., Muggeridge, A.H., Goode, A.T. *et al*.: "Effective History Matching: The Application of Advanced Software Techniques to the History Matching Process," paper SPE 25250 presented at the 1993 SPE Reservoir Simulation Symposium, New Orleans, Louisiana, February 28-March 3.
7. Eide, A.L., Holden, L., Reiso, E. and Aanonsen, S.I.: "Automatic History Matching by Use of Response Surface and Experimental Design," paper presented at the 1994 IV European Conference on Mathematics of Oil Recovery, Roras, Norway, June 7-10.

8. Zabala, I., Blanc, G., Collombier, D. and Mezghani, M.: "Use of Experimental Design in Resolving Inverse Problems: Application to History Matching", paper presented at the 2000 VII European Conference on Mathematics of Oil Recovery, Baveno, Italy, September 5-8.
9. Zabala, I.M. and Mezghani, M.: "Constraining Reservoir Facies Models to Dynamic Data-Impact," paper SPE 71335 presented at the 2001 SPE Annual Technical Conference and Exhibition, New Orleans, Louisiana, September 30-October 3.
10. Damsleth, E., Hage, A. and Volden, R.: "Maximum Information at Minimum Cost: A North Sea Field Development Study Using Experimental Design," paper SPE 23139 presented at the 1991 Offshore Europe Conference, Aberdeen, Scotland, September 3- 6.
11. Faidi, S.A., Ponting, D.K. and Eagling, T.L.: "Experimental Design in Interactive Reservoir Simulation," paper SPE 36005 presented at the 1996 Petroleum Computer Conference, Dallas, Texas, June 2- 5.
12. Dejean, J.P. and Blanc, G.: "Managing Uncertainties on Production Predictions Using Integrated Statistical Methods," paper SPE 56696 presented at the 1999 SPE Annual Technical Conference and Exhibition, Houston, Texas, October 3-6.
13. Venkataraman, R.: "Application of the Method of Experimental Design to Quantify Uncertainty in Production Profiles," paper SPE 59422 presented at the 2000 Asia Pacific Conference on Integrated Modeling for Asset Management, Yokohama, Japan, April 25-26.
14. Chewaroungroaj, J., Varela, O.J. and Lake, L.W.: "An Evaluation of Procedures to Estimate Uncertainty in Hydrocarbon Recovery Predictions," paper SPE 59449 presented at the 2000 Asia Pacific Conference on Integrated Modeling for Asset Management, Yokohama, Japan, April 25-26.
15. Elk, J.F., Guerrera, L., Vijayan, K. and Gupta, R.: "Improved Uncertainty Management in Field Development Studies Through the Application of the Experimental Design Method to the Multiple Realizations Approach," paper SPE

64462 presented at the 2000 SPE Annual Technical Conference and Exhibition, Dallas, Texas, October 1-4.

16. Corre, B., Feraudy, V. and Vincent, G.: "Integrated Uncertainty Assessment for Project Evaluation and Risk Analysis," paper SPE 65205 presented at the 2000 European Petroleum Conference, Paris, France, October 24-25.
17. King, M.J. and Datta-Gupta, A.: "Streamline Simulation: A Current Perspective*," In Situ* (1998) **22**, No.1, 91-140.
18. Idorobo, E.A., Choudhary, M.K. and Datta-Gupta, A.: "Swept Volume Calculations and Ranking of Geostatistical Reservoir Models Using Streamline Simulation," paper SPE 65557 presented at the 2000 AAPG Western Regional Meeting, Long Beach, California, June 19-23.
19. Zang, T.A. and Green, L.L.: "Multidisciplinary Design Optimization Techniques: Implications and Opportunities for Fluid Dynamics Research," paper AIAA-99-3708 presented at the 1999 30th AIAA Fluid Dynamics Conference, Norfolk, Virginia, June 28-July 1.
20. Toropov, V.V. and Alvarez, L.F.: "Application of Genetic Programming and Response Surface Methodology to Optimization and Inverse Problems," paper presented at the 1998 Inverse Problems in Engineering Mechanics, Nagano-shi, Japan, March 24-27.
21. Rikards, R.: "Method of Identification of Elastic Properties of Laminates Based on Experiment Design," *Composites: Part B* (1999) **30**, 279-289.
22. Bates, R. A., Buck, R.J., Riccomango, E. and Wynn, H.P.: "Experimental Design and Observation for Large Systems*," J. of the Royal Statistical Society*. (1996) **58**, No.1, 77-94.
23. Sacks, J., Welch, W.J., Mitchell, T.J. and Wynn, H.P.: "Design and Analysis of Computer Experiments," *Statistical Science* (1989) **4**, No.4, 409-435.
24. Myers, R.H. and Montgomery, D.C.: *Response Surface Methodology: Process and Product Optimization Using Designed Experiments*, Wiley, New York (1995), 700.

25. Box, G.E.P. and Draper, N.R.: *Empirical Model Building and Response Surfaces*, Wiley, New York (1987), 699.
26. Box, G.E.P. and Behnken, D.W.: "Some New Three Level Designs for the Study of Quantitative Variables," *Technometrics* (1960) **2**, No.4, 455.
27. Fox, M.J., Chedburn, A.C.S. and Stewart, G.: "Simple Characterization of Communication Between Reservoir Regions," paper SPE 18360 presented at the 1998 SPE European Petroleum Conference, London, UK, Oct. 16-19.
28. Ursin, J-R.: "Fault Block Modelling-An Alternative Simulation Tool for Strongly Compartmentalized Gas Reservoirs," *JCPT*, (Nov. 2001) **40**, 42-49.
29. Hagort, J. and Hoogstra, R: "Numerical Solution of the Material Balance Equations of Compartmented Gas Reservoir," *SPE Reservoir Eval. & Eng*. (Aug 1999) 385.
30. Ehllg-Economides, C.A.: "Application for Multiphase Compartmentalized Material Balance," paper SPE 27999 presented at the Univ. Of Tulsa Centennial Petroleum Engineering Symposium, Tulsa, OK, Aug. 29-31, 1994.
31. Stewart, G. And Whaballa, A.E.: "Pressure Behaviour of Compartmentalized Reservoirs," paper SPE 19779 presented at the 1989 SPE Annual Technical Conference and Exhibition, San Antonio, Texas, Oct. 8-11.
32. Rahman, N.M.A. and Ambastha, A.K.: "Generalized 3D Analytical Model for Transient Flow in Compartmentalized Reservoir," *SPEJ* (Sept. 2001) 276.
33. Palacio, J.C. and Blasingame, T.A.: "Decline Curve Analysis Using Type Curves: Analysis of Gas Well Production Data," paper SPE 25909 presented at the 1993 Rocky Mountain Regional/Low Permeability Reservoir Symposium, Denver, Colorado, April 12-14.
34. Doublet, L.E., Pande, P.K., McCollum, T.J. and Blasingame, T.A.: "Decline Curve Analysis Using Type Curve-Analysis of Oil Well Production Using Material Balance Time: Application to Field Case," paper SPE 28688 presented at the 1994 SPE Petroleum Conference and Exhibition of Mexico, Veracruz, Mexico, Oct. 10-13.

35. Kulkarni, K.N., Datta-Gupta, A. and Vasco, D.W.: "A Streamline Approach for Integrating Transient Pressure Data Into High –Resolution Reservoir Models," *SPEJ* (September 2001) 273.
36. Deutsch, C.V and Wang, L.: "Hierarchical Object-based Stochastic Modeling of Fluvial Reservoirs," *Mathematical Geology* (1996) **28**, No.7, 857.
37. Deutsch, C.V and Tran, T.T.: "FLUVSIM: A Program for Object-Based Stochastic Modeling of Fluvial Depositional Systems," *Computers and Geosciences* (2002) **28**, 525.
38. Pollock, D.W.: "Semianalytical Computation of Pathlines for Finite-Difference Models," *Groundwater* (1988) **26**, No.6, 743.
39. Virieux, J., Flores-Luna, C. and Gibert, D.: "Asymptotic Theory for Diffusive Electromagnetic Imaging," *Geophys. J. Int*. (1994) **119**, 857
40. Imam, R. L and Conover, W.J.: "Small Sample Sensitivity Analysis Techniques for Computer Models, With an Application to Risk Assessment," *Commun. Stat.- Theor. Meth.* (1980), **17**, No.A9, 1749.
41. Lentner, B. and Bishop, T.: *Experimental Design and Analysis*, Valley Book Company, Blacksburg, Virginia (1993), 90.

APPENDIX A

SAS INPUT TO PERFORM THE SNK AND TUKEY MEAN SEPERATION TESTS

```
TITLE 'DRAINAGE VOLUME: 7 LOCATIONS';
CARDS;
1  1 16.92
1  2 17.05
1  3 16.94
1  4 17.10
1  5 16.93
1  6 16.98
1  7 17.05
2  1 16.89
2  2 16.89
2  3 16.89
2  4 16.94
2  5 16.92
2  6 16.91
2  7 16.92
3  1 18.19
3  2 18.18
3  3 18.19
3  4 18.18
3  5 18.17
3  6 18.19
3  7 18.17
4  1 11.24
4  2 11.18
4  3 12.89
4  4 13.31
4  5 13.54
4  6 13.71
4  7 13.93
5  1 12.45
5  2 14.17
5  3 13.89
5  4 13.89
5  5 13.94
5  6 14.18
5  7 14.47
6  1 10.57
```

```
6  2 11.03
6  3 11.03
6  4 12.35
6  5 12.99
6  6 13.29
6  7 13.41
7  1 10.81
7  2 12.07
7  3 13.03
7  4 13.37
7  5 13.54
7  6 13.88
7  7 13.98
8  1 17.02
8  2 17.04
8  3 17.02
8  4 17.03
8  5 17.03
8  6 17.03
8  7 17.04
9  1 16.51
9  2 16.68
9  3 16.71
9  4 16.84
9  5 16.47
9  6 16.43
9  7 16.47
10 1 15.72
10 2 15.74
10 3 16.84
10 4 15.33
10 5 15.18
10 6 14.74
10 7 14.99
PROC GLM;
CLASS TRANS LOCATION;
MODEL DRAIN=TRANS LOCATION/SS3;
MEANS LOCATION;
MEANS TRANS;
MEANS TRANS/SNK TUKEY;
MEANS LOCATION/SNK TUKEY;
```

APPENDIX B

RESPONSE SURFACE GENERATION USING EREGRESS SOFTWARE

Essential experimental design and regression software (EREGRESS)

- Initialize the macros *Eed22.xla* and *Eer22.xla* and open an EXCEL sheet
- Go to DOE (Design of Experiment) and select Design an Experiment.
- Select the number of factors, the number of responses, the type of response surface design and finally the number of centerpoints
- Choose the Factor names, select the highest and lowest factor levels and choose units each factor.
- Once the experimental design is set up completely with response values, perform regression using Analyze Design. The following interface can be seen for pixel-based regression:

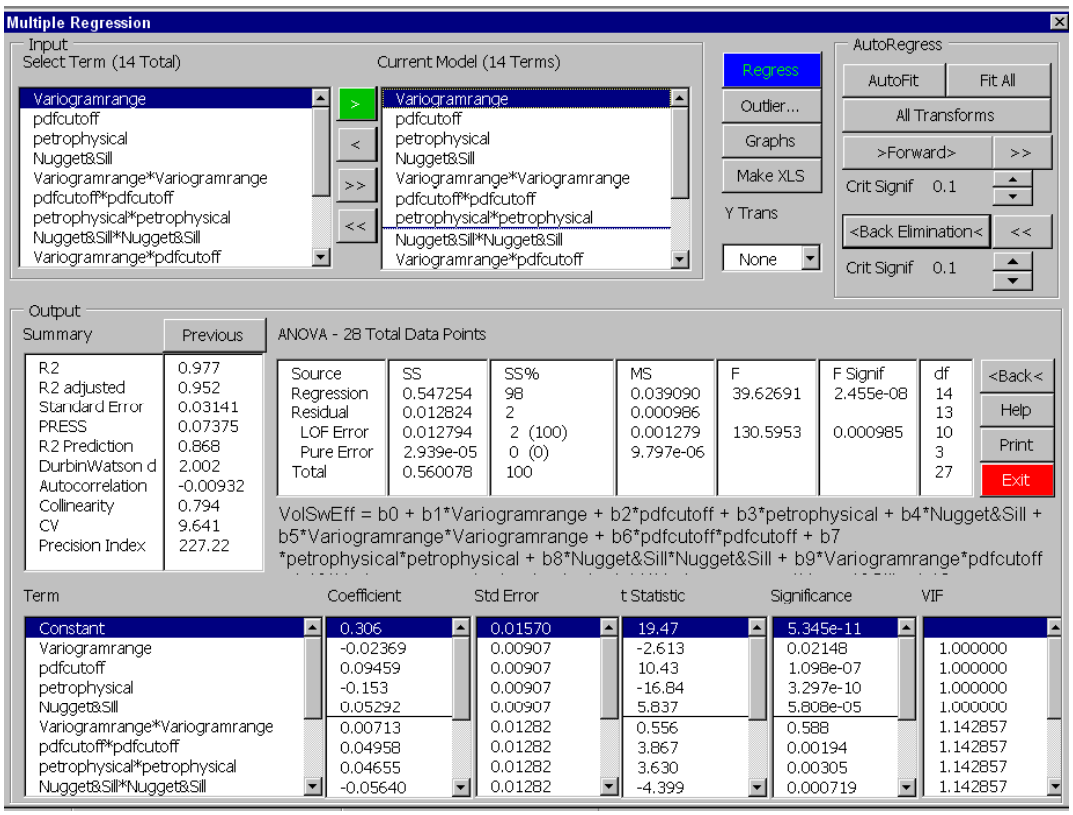

- Select the parameter terms, quadratic terms and the interaction terms for the response surface model and click on MAKE XLS button to generate an EXCEL sheet with response surface results.

VITA

Harshal Parikh received his B.S. degree in chemical engineering from Mumbai University Institute of Chemical Technology, India, in May 2000. His experience includes working as a Graduate Research Assistant in the Reservoir Characterization group with Dr.Akhil Datta-Gupta and an internship with Ambuja Cements Pvt.Ltd in the field of process design and optimization.

His current address: 9200 N. Plaza Drive
Apt # 3109
Austin, Texas 78753
USA